SEDIMENTOLOGY the journal of the International Association of Sedimentologists

Sedimentology (2010) **57,** 1–26 doi: 10.1111/j.1365-3091.2009.01109.x

Fluvial and submarine morphodynamics of laminar and near-laminar flows: a synthesis

ERIC LAJEUNESSE*, LUCE MALVERTI*, PIERRE LANCIEN*, LAWRENCE ARMSTRONG*, FRANCOIS MÉTIVIER*, STEPHEN COLEMAN†, CHARLES E. SMITH‡, TIMOTHY DAVIES§, ALESSANDRO CANTELLI¶ and GARY PARKER¶

**Equipe de Dynamique des Fluides Géologiques, Institut de Physique du Globe de Paris, Paris, France (E-mail: lajeunes@ipgp.jussieu.fr)*

†Department of Civil & Environmental Engineering, The University of Auckland, Auckland, New Zealand

‡Department of Mechanical Engineering, Virginia Tech University, Blacksburg, VA 24060, USA

§Department of Geological Sciences, University of Canterbury, Christchurch, New Zealand

¶Department of Civil & Environmental Engineering and Department of Geology, University of Illinois, Urbana, IL 61801, USA

Associate Editor – Steve Rice

ABSTRACT

The interaction of flow with an erodible bed in alluvial rivers and deep-sea channels gives rise to a wide range of self-formed morphologies, including channels, ripples, dunes, antidunes, alternate bars, multiple-row bars, meandering and braiding. As the flow is invariably turbulent in field manifestations of these morphologies, there has been a tendency to assume that turbulence is necessary for them to form. While turbulence undoubtedly has an important influence when it is present, it is not necessary for any of these features. Indeed, all of these features can be formed by the morphodynamic interaction of purely laminar or nearly laminar flow with an erodible bed. This paper provides a survey and synthesis of a wide range of laminar or near-laminar flow analogues of morphologies observed in the field. Laminar-flow analogues of turbulent-flow morphologies cannot and should not be expected to satisfy dynamic similarity in terms of all relevant dimensionless parameters. What is of more significance is the convergence of the underlying physics. It is illustrated in this paper that many existing theoretical frameworks for the explanation of turbulent-flow morphodynamics require only relatively minor modification in order to adapt them to laminar flows.

Keywords Fluvial and submarine morphodynamics, laminar flow, micro-scale modelling, river bedform, turbulent flow.

INTRODUCTION

Alluvial rivers self-construct their channels from their own sediment, developing rhythmic morphologies such as ripples, dunes, antidunes, single-row and multiple-row bars, and forming both meandering and braiding planforms. Turbulence being ubiquitous in alluvial rivers, it is thus reasonable to assume that turbulence is associated closely with these morphologies (e.g. Nezu & Nakagawa, 1993). Indeed, turbulence has been assumed by many researchers to be a causative agent of many of these bedform morphologies, through the role of coherent structures (e.g. Yalin, 1992; Yalin & da Silva, 2001; da Silva, 2006).

In this paper, examples are reviewed demonstrating the ability of laminar flow to generate morphodynamic features similar to those generally associated with turbulent flow. Turbulence does play an important role when it is present. However, the fact that so many distinct fluvial morphologies can be created by laminar flow suggests that: (i) the role of turbulence cannot be essential for the morphologies themselves; and

(ii) microscale experiments with laminar flow provide a useful way to create analogues of morphodynamic phenomena that also occur in turbulent flow at field scales. These conclusions are illustrated through many examples gleaned from published papers, recent doctoral theses, a technical report and new results reported here.

It should be emphasized that the present study does not argue for a superficial resemblance between laminar and turbulent morphodynamic features but for analogous forms that derive from a convergence in the underlying physics. This convergence does not require the satisfaction of strict dynamic similarity in all dimensionless parameters. Indeed, illustrating that such analogous forms exist and have common physical underpinnings, in spite of the absence of dynamic similarity, is the objective of this paper.

Firstly, the definitions and properties of laminar and turbulent flow are recalled briefly, followed by an enumeration of many examples of morphologies created by laminar and near-laminar flows, along with their turbulent-flow counterparts; this is carried out with a minimum of interpretation in order to first establish the range of analogous morphologies. Secondly, a specific example is considered, i.e. secondary flow in bends. This example is used to show that turbulent-flow phenomena can have laminar-flow analogues that derive from the same physics, even though dynamic similarity is not satisfied. Thirdly, how a number of existing morphodynamic models designed to describe turbulent-flow morphologies can be adapted in a straightforward manner to encompass their laminar analogues is indicated. Finally, a discussion of the role of turbulence in erodible-bed morphodynamics provides a conclusion.

LAMINAR VERSUS TURBULENT FLOW

Turbulent flow is characterized by random but correlated fluctuations in both space and time around a mean flow which may itself be non-uniform and/or unsteady. Wall-bounded turbulent flows (such as in a river, where the walls are the bed and banks) are associated with large Reynolds numbers (as defined below) and include: (i) random and unpredictable components of the flow field; (ii) three-dimensional fluctuations; and (iii) energy dissipation rates and rates of diffusion (dispersion) of mass, heat, momentum, energy, etc., which are well in excess of those that would prevail in the absence of turbulence (e.g. Tennekes & Lumley, 1972; Kantha & Clayton, 2000). Turbulent flows generate free eddies which, while having considerable random components, nevertheless often organize themselves into structures with measurable degrees of coherence (e.g. Nezu & Nakagawa, 1993). The existence of these structures, which was first determined based on experiments and field observations (see, for example, Ashworth *et al.*, 1996 for several field descriptions), has been verified in recent years by means of direct numerical simulation (e.g. Kantha & Clayton, 2000). Turbulent flows are thus a mixture of random and coherent structures, with the latter suppressed at the smallest scales.

The type of turbulence considered here, i.e. wall-bounded turbulence, was first studied in terms of steady, streamwise-uniform flow in round pipes. Consider a pipe of diameter D_p containing a fluid with a viscosity ν and a cross-sectionally averaged flow velocity U. Pope (2000) makes the following observation: ''As Reynolds (1894) noted, the flow is characterized by a single, non-dimensional parameter, now known as the Reynolds number…''. Here this Reynolds number is termed Re_{pipe}:

$$Re_{pipe} = \frac{UD_p}{\nu} \tag{1}$$

Pope (2000) continues as follows: ''In Reynold's pipe-flow experiment, if Re_{pipe} is less than 2300, the flow is laminar… If, on the one hand, Re_{pipe} exceeds 4000, then the flow is turbulent. The range $2300 \leq Re_{pipe} \leq 4000$ defines a transitional range from fully laminar to fully turbulent flow.'' (In the above quotes, the original notation used by Pope for the Reynolds number has been replaced with that defined above.)

The translation of the above result to more general geometries of steady, streamwise-uniform flow in pipes and open channels is made straightforward by the use of the hydraulic radius r_H. This parameter is defined to be the cross-sectional area of flow divided by the wetted perimeter (e.g. Reynolds, 1974). In the case of a pipe, r_H takes the form:

$$r_H = \frac{\pi(D_p/2)^2}{\pi D} = \frac{D_p}{4} \tag{2}$$

Based on the above-quoted results, a generalized set of criteria for such flows can be stated using the corresponding Reynolds number:

$$Re = \frac{Ur_H}{\nu} \tag{3}$$

The flow is laminar when:

$$Re < 575 \tag{4a}$$

transitional when:

$$575 \leq Re < 1000 \tag{4b}$$

and fully turbulent when:

$$Re \geq 1000 \tag{4c}$$

The archetypal geometry for consideration here is steady, streamwise-uniform (at large-scale) open-channel flow in a rectangular channel with depth H and width B. It is further assumed that the flow is shallow in the sense that $H/B \ll 1$. The relevant form for hydraulic radius r_H for wide open-channel flow is:

$$r_H = \frac{BH}{B+2H} = \frac{H}{1+2(H/B)} \cong H \tag{5}$$

The relevant form for the Reynolds number is thus obtained by the transformation $r_H \rightarrow H$ in Eq. 3, so that:

$$Re = \frac{UH}{\nu} \tag{6}$$

The research which is synthesized herein focuses specifically on cases for which $Re < 575$. Also included are some flows for which $575 \leq Re < 1000$, i.e. transitional or nearly laminar flows.

The Reynolds number is often interpreted as a scale for the ratio of inertial force (the force that would be necessary to bring a given flow to a halt) to the viscous force. Highly viscous flows are characterized by a Reynolds number that is much smaller than unity. It is emphasized here that in the case of open-channel flow, however, flow in the range $1 < Re < 575$ is inertially dominated yet laminar; this means that, at the scale at which eddies can be internally generated, viscosity dominates the flow. Indeed, a fundamental area of fluid mechanics, boundary layer theory, was developed by Prandtl (Schlichting, 1968) for the case of high Reynolds number, yet laminar flow over a flat plate.

Finally, two additional points are emphasized. Firstly, once turbulence develops, it creates effectively its own enhanced viscosity. Using Eq. 6 and a conventional turbulent (eddy) viscosity $\nu_T = \kappa u_* H$, provides an effective turbulent Reynolds number value of $\sqrt{c_f}/\kappa$ where u_* is the shear velocity, κ is the Von Kármán constant and c_f is the friction coefficient of the turbulent flow (see Eq. A7 in the *Appendix*).

Secondly, it is necessary to point out that laminar flows are not necessarily eddy-free flows. An example of particular relevance herein is the case of eddies forced by curvature. It has been known since the time of Rozovskii (1961) that channel planform curvature drives the eddy pattern known as secondary flow in river bends. River flow invariably is turbulent; the curvature-driven eddy pattern is superimposed over this turbulence. This same eddy pattern, however, occurs for identical reasons in laminar flow in pipes.

Curvature-driven eddies in laminar flow were first considered in the context of flow in a pipe twisted into a spiral configuration (e.g. Dean, 1928). These eddies are mediated by the dimensionless number known as the Dean number, De, which can be defined as:

$$\mathrm{De} = \frac{1}{2} Re_{\mathrm{pipe}} \left(\frac{D_p}{2R_c} \right)^{1/3} \tag{7}$$

where R_c denotes the curvature of the spiral path of the pipe.

In a similar way, flow confluences, constrictions and sudden changes in flow direction can also generate forced eddies, regardless of whether the flow itself is laminar or turbulent. In the case of water–sediment interaction, the interaction itself can create the morphologies necessary to spawn forced eddies, which then can interact with the evolving boundary.

EXAMPLES OF LAMINAR-FLOW MORPHOLOGIES AND PHENOMENA AND THEIR TURBULENT-FLOW ANALOGUES

In this section it is demonstrated that bedload transport associated with turbulent flow has a laminar-flow analogue. It is then shown that the following analogues of river morphologies can be created under conditions of laminar or nearly laminar flow: self-formed channels, dunes/ripples, single-row and multiple-row alternate bars, meandering and braiding. In conclusion, it is illustrated that submarine canyons and levéed submarine channels also have laminar analogues.

Bedload transport relation for laminar flow

The creation of bed morphologies of the type under consideration requires the erosion, trans-

port and deposition of bed sediments. Turbulent flows can transport bed sediment as both bedload, consisting of particles that roll, slide and saltate near the bed, and suspended load, consisting of particles that are wafted upward and away from the bed by turbulence. A plethora of predictive relations are available for the description of bedload and suspended load transport by turbulent flow (e.g. Garcia, 2008). Laminar flows, by contrast, can transport sediment only as bedload. Laminar forced eddies can, of course, suspend sediment, and sediment in antecedent suspension can be carried by laminar flow. However, in both these cases, laminar transport of 'suspended' sediment lasts only for the time necessary for sediment to settle down. Sustained, equilibrium transport of sediment in suspension is not possible in the case of steady, uniform, rectilinear laminar flows due to the absence of the free eddies necessary to entrain sediment into suspension. The bulk of laminar-flow morphologies therefore are associated with the differential transport of sediment moving as bedload.

The best-known relation for bedload transport under turbulent conditions is that of Meyer-Peter & Müller (1948). Here a corrected form due to Wong & Parker (2006) is presented. The relation was determined empirically using data with values of Re ranging from $1{\cdot}7 \times 10^4$ to $2{\cdot}3 \times 10^6$, i.e. well into the range of fully turbulent flow. Let q_b denote the volume bedload transport rate per unit width, ρ and ρ_s denote the material density of water and sediment, respectively, τ_b denote bed shear stress, D characteristic sediment grain-size and g gravitational acceleration. The following dimensionless parameters can be formed from these; the submerged specific gravity of the sediment R, given as:

$$R = \frac{\rho_s}{\rho} - 1 \tag{8}$$

and the dimensionless Einstein and Shields numbers, defined, respectively, as:

$$q_b^* = \frac{q_b}{\sqrt{RgD}D}, \quad \tau^* = \frac{\tau_b}{\rho RgD} \tag{9a,b}$$

The bedload transport equation of Meyer–Peter and Müller as corrected by Wong & Parker (2006) takes the following form for the case of flow over a plane bed (no bedforms):

$$q_b^* = 4(\tau^* - \tau_{ce}^*)^{3/2}, \quad \tau_{ce}^* = 0{\cdot}0495 \tag{10a,b}$$

where τ_{ce}^*denotes an effective 'critical' Shields number below which bedload transport is negligible. Meyer-Peter & Müller (1948) and Wong & Parker (2006) used τ_{ce}^* as a fitting parameter, but the former authors provide information suggesting that a more accurate estimate of the critical Shields number τ_c^* at the threshold of motion is about 0·03.

Malverti *et al.* (2008) recently determined a corresponding relation for bedload transport by laminar flow based on experimental data. Details of the experiments can be found in the original reference. A brief summary, however, is given here to demonstrate the range of conditions associated with laminar morphodynamics.

The experiments were conducted in a rectangular flume, with a width B = 6 cm and lengths L of either 40 or 80 cm. The bed was covered with loose sediment consisting of glass beads of submerged specific gravity R = 1·45. The median grain size D_{50} was 75 μm, D_{10} and D_{90} being 50 and 90 μm, respectively. For each experiment, flow discharge Q was maintained at a constant value. No sediment was fed into the channel during the experiments. The experiment duration was so short, however, that: (i) the change in channel slope S in the measuring reach was not significant; and (ii) the effect of sediment starvation at the entrance did not have time to propagate far enough downstream to influence conditions in the measuring reach. Sediment, entrained as bedload by the flow, was collected and weighed in a tank at the downstream end of the flume.

The flow velocity U_{max} at the water surface was measured by tracking the motion of small floating plastic tracer particles entrained by the flow (Armstrong, 2003). The depth-averaged flow velocities U were inferred using the assumption of laminar flow, according to which:

$$U = \frac{2}{3} U_{max} \tag{11}$$

The values so obtained fell in the range of 6·8 to 28 cm sec^{-1}. The corresponding flow depths H estimated from continuity:

$$H = \frac{Q}{BU} \tag{12}$$

varied between 0·11 and 0·30 cm.

The Reynolds number Re ranged from 138 to 555, so that all experimental flows satisfied Criterion 4a therefore being laminar. The flows were also observed to satisfy normal flow conditions so that the streamwise bed shear stress could be calculated from the following relation:

$$\tau_b = \rho g H S \tag{13}$$

The Shields stress τ^* was then computed from Eqs 9b and 13 as:

$$\tau^* = \frac{HS}{RD} \tag{14}$$

Here D refers to the median size D_{50} quoted above.

The bedload transport relation determined by Malverti *et al.* (2008) from this set of experiments has the form:

$$q_b^* = 0 \cdot 67(\tau^* - \tau_{ce}^*)^{3/2}, \quad \tau_{ce}^* = 0 \cdot 12 \tag{15a,b}$$

where τ_{ce}^* again represents a fitting parameter. The above relation is plotted along with the data in Fig. 1. Also included in the plot is Eq. 10a,b, i.e. the Wong & Parker (2006) corrected version of the relation of Meyer-Peter & Müller (1948). Except for the values of the coefficients, Eq. 15a,b which governs bedload transport in a laminar river is similar in shape to the Meyer-Peter & Müller (1948) transport model for turbulent flows (Eq. 10a,b). In particular, both relations have the same exponent, 3/2.

Self-formed channels with mobile bed and stable banks

When subjected to a set flow regime, rivers progressively evolve toward a state at which they are capable of transporting the alluvium of which they are made without changing average channel cross-sectional geometry or slope over time (e.g. Parker, 1978). In that dynamic equilibrium state, the average channel width and depth remain constant and sediment is transported continuously over the bed, but net bank erosion is negligible This fundamental process has been modelled largely in the frame of turbulent flow laboratory experiments (e.g. Ackers, 1964; Ikeda, 1981; Diplas, 1990; Macky, 1999; to name only a few). An example of such a channel formed by turbulent flow (*Re* in the range of 6800 to 14 500) is shown in Fig. 2 (Diplas, 1990).

The same process of self-forming of a mobile-bed equilibrium channel has been modelled in a purely laminar flow by Armstrong (2003). The experiments in question were very similar to those of Malverti *et al.* (2008), but both the bed and banks were freely erodible. The sediment was well-sorted silica beads with $D_{50} = 75$ μm, $D_{90} = 90$ μm and $R = 1{\cdot}49$. In performing the experiments, a narrow rectangular channel of initial width 3 to 4 cm was excavated first, and then allowed to widen freely under the action of a flow (Fig. 3). The length of the experimental reach was 1·1 m. Flow discharge Q varied from $8{\cdot}33 \times 10^{-6}$ to $2{\cdot}17 \times 10^{-5}$ m^3 sec^{-1} and bed slope S varied from 0·017 to 0·052. The channel water surface width B at mobile-bed equilibrium was measured photographically and found to range from 2·5 to 8·4 cm. The flow velocity

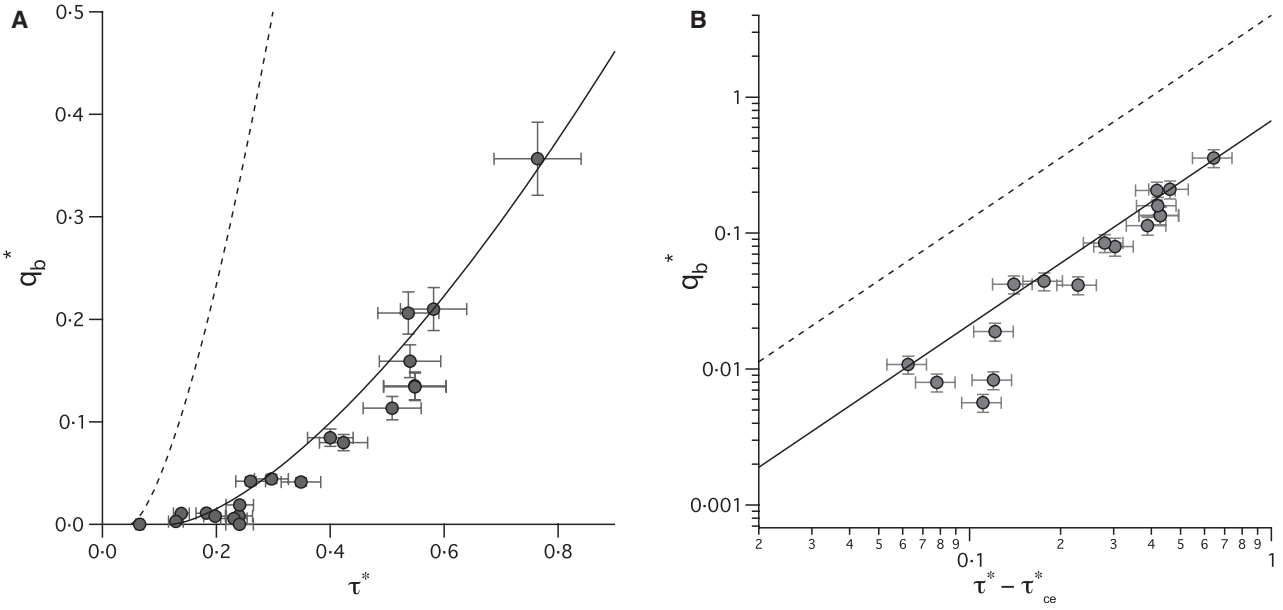

Fig. 1. Plot of the Einstein number q_b^* versus (A) the Shields number and (B) the excess Shields number. Circles correspond to data acquired by Malverti *et al.* (2008) for a laminar flow in flumes with lengths of 40 and 80 cm. The plain line corresponds to Eq. 15a,b fitted to the laminar data. The dotted line corresponds to Eq. 10a,b representing the Wong & Parker (2006) corrected version of the relation of Meyer-Peter & Müller (1948).

Fig. 2. Image of a stable self-formed mobile-bed channel in fine gravel. The width of the channel is about 29 cm. The flow, which was from bottom to top, has been turned off. The image is courtesy of P. Diplas.

U_{max} at the water surface was evaluated within an uncertainty of 10% by tracking the motion of small floating tracer plastic particles entrained by the flow. The velocity was deduced by measuring the distances covered by particles between two consecutive images. U_{max} varied in the range 13·4 to 67·7 cm sec^{-1}; the range of depth-averaged flow velocity U, inferred from these numbers and Eq. 11, is 8·9 to 45·1 cm sec^{-1}. Flow depths H computed from Eq. 12 within an uncertainty of 10% ranged from 0·065 to 0·25 cm. The aspect ratio B/H ranged from 10 to 113, with an average value of 51, so confirming that all the channels were wide. The Froude number Fr of the flow defined as:

$$Fr = \frac{U}{\sqrt{gH}} \tag{16}$$

was estimated within an uncertainty of 15%. It was found to range from 0·84 to 3·8. However, the flow was Froude-subcritical ($Fr < 1$) in only a single case.

Most importantly, the Reynolds number Re ranged from 95 to 790, with an average value of 309. The database compiled by Armstrong (2003) contains the results of 53 experiments. In only four of the 53 cases did Re equal or exceed Criterion 4a; the flow in the remaining 49 experiments could thus be classified as laminar.

The time evolution of a mobile-bed 'microchannel' formed during one of the Armstrong (2003) experiments is shown in Fig. 3. The channel formed by the laminar flow is only a few centimetres in width and a few millimetres in depth. It nevertheless exhibits the same general features as its self-formed equivalent created by turbulent flow: progressive widening of the channel until a dynamic equilibrium state is reached, characterized by constant channel width and depth and continuous sediment transport over the bed with no net bank erosion.

The extensive data set assembled by Armstrong not only demonstrates the ability of laminar flows to create self-formed channels, but it also allows for testing of a number of hypotheses concerning self-formed channels associated with laminar flows. These issues are considered in more detail after surveying the full range of laminar-flow morphologies.

Dunes/ripples and antidunes in laminar flow

Ripples and dunes are the standard bedforms of lower regime flow (Vanoni, 1974; Garcia, 2008). These bedforms typically have gently sloping stoss (upstream) sides and steeply sloping lee sides, and invariably migrate downstream (Fig. 4A). Water surface undulations are either weak, and out of phase with bed undulations, or absent. The corresponding upper-regime bedform is the antidune. Antidunes may migrate upstream, in which case they tend to be rather symmetrical, or downstream, in which case they often have the same asymmetric shape as dunes (Foley & Vanoni, 1977; Carling *et al.*, 2005). Water surface undulations are strong and are in phase with bed undulations.

The terms 'lower regime' and 'upper regime' merit some clarification. Loosely speaking, lower regime corresponds to Froude-subcritical flow ($Fr < 1$) and upper regime corresponds to Froude-supercritical flow ($Fr > 1$). The theoretical analyses of Anderson (1953) and Kennedy (1963), however, show that when the wavelength of a bedform is sufficiently small compared with flow depth, the flow can respond in a Froude-supercritical way even when Fr is modestly smaller than unity. This result corresponds with the data analysis of Vanoni (1974).

Dunes formed under conditions of turbulent flow are illustrated in Fig. 4A for the Mississippi

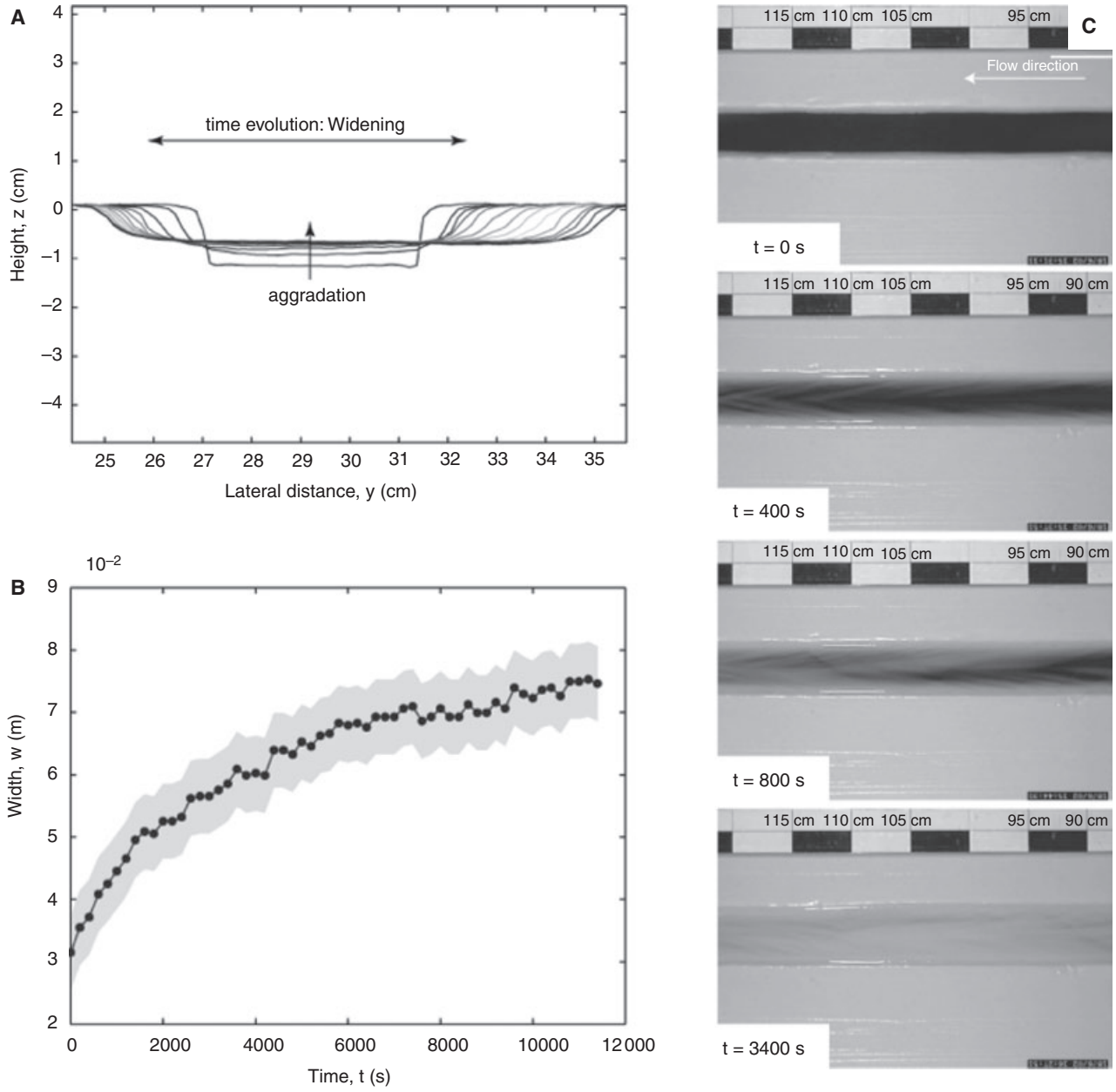

Fig. 3. Time evolution of a channel formed in mobile-bed laminar microscale river by Armstrong (2003). The experimental sediment consists of glass beads of mean diameter 75 μm. (A) Channel section profiles every 300 sec at x = 100 cm from the inlet. (B) Evolution of the width of the river as a function of time. The river enlarges until an equilibrium is reached. (C) Images showing the evolution of the microscale laminar river. At the beginning of the experiment, the central channel is not covered by sediments so that the flume bottom (painted in black) is exposed. Once the flow is initiated, the channel is progressively covered by sediments eroded from the banks.

River, for which Reynolds numbers are of the order of 10^7. Figure 4B illustrates analogous bedforms created under conditions of laminar flow. The bedforms in question, which are documented in Coleman *et al.* (1998) and Coleman and Eling (2000), migrated downstream and possessed gentle stoss and steep lee faces, and thus could be classified as either dunes or ripples.

The precise criterion distinguishing dunes from ripples remains the subject of some debate. Liu (1957) and Engelund & Hansen (1967), for example, suggest that ripples form from an antecedent condition for which a viscous sublayer separates the bed from the turbulent flow above, and dunes form from an antecedent condition for which the viscous sublayer is absent. In the case of laminar flow, the flow is viscous across the entire depth,

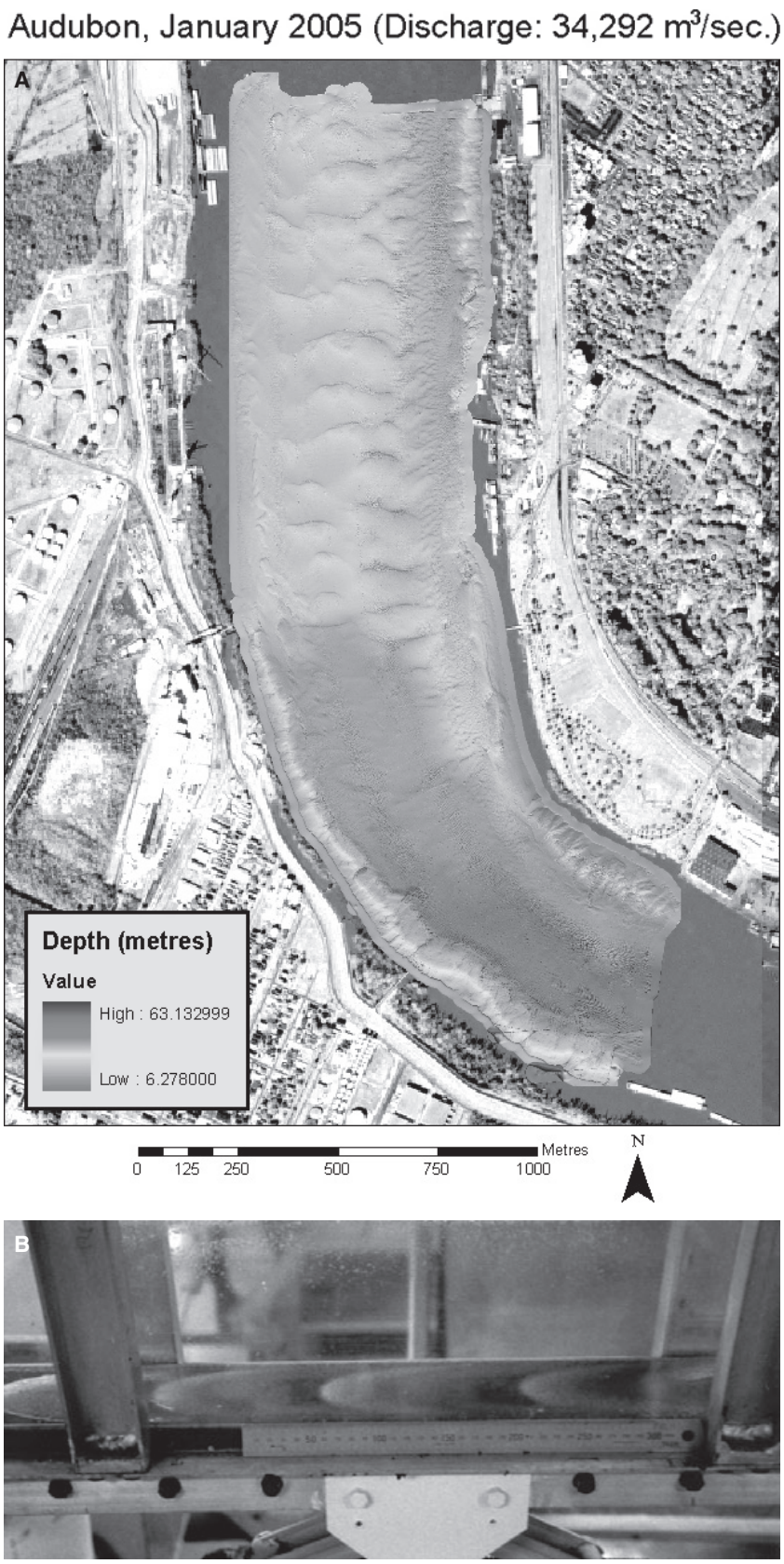

Fig. 4 (A) Acoustic image of dunes in the Mississippi River at New Orleans during a flood flow in January 2005. Flow is from top to bottom. The image is courtesy of M. Allison and J. Nittrouer. (B) Oblique plan view of wavelets formed under laminar flow conditions in the experiments of Coleman & Eling (2000). Flow was from right to left. The value of the Reynolds number is Re = 169.

so such a discrimination would break down. Coleman *et al.* (1998) and Coleman & Eling (2000) sidestep the issue of ripples versus dunes by describing their bedforms as 'sand wavelets'.

The above experiments were carried out in a tilting flume with glass sidewalls measuring 0·3 m × 0·1 m (wide) × 2·55 m (long), with a header tank at the inlet and a collection bay at the outlet. A full-width recess in the wooden channel base measuring 0·025 m (deep) × 1·3 m (long) was filled with sand (R = 1·65) to create an erodible-bed section for the tests. Flows were set using a pump. The fluid was Shell Tellus Grade 32 hydraulic oil (ρ = 870 kg m^{-3}). At the start of each experiment the bed was smoothed, the settings for the desired flow were established and then the flow was initiated. Sediment was not recirculated. At selected stages of bed development, the flow was halted and centreline bed elevations were measured beneath the oil to within ±0·4 mm every 1·2 mm along the flume. After a bed profile was recorded, the flow was then either resumed in the channel or the bed was flattened with the experiment being started from the beginning and run to a later stage of development.

Coleman & Eling (2000) and Coleman *et al.* (1998) generated sand wavelets for eight uniform-flow tests with ν = 0·80 to 1·00 × 10^{-4} m^2 sec^{-1} (varying with oil temperature), D = 0·28 to 0·44 mm, H = 0·038 to 0·068 m, U = 0·273 to 0·519 m sec^{-1}, Fr = 0·40 to 0·63 (subcritical), Re = 116 to 441 (laminar flow) and τ^*/τ_c^* = 1·6 to 8·8 (so that sediment was in transport). The pattern of sand wavelet generation downstream of a discontinuity in the bed for these flows was found to be consistent with observed patterns for turbulent alluvial flows. Wavelet profiles (see Fig. 4B) and lengths were further found to be comparable with those for turbulent alluvial flows. Sand wavelets were also observed to grow from an initially flat surface for closed-conduit (piped) laminar flows (Kuru *et al.*, 1995). The similar natures of these nascent wavelets for closed-conduit and open-channel laminar and turbulent flows are demonstrated in Coleman *et al.* (2003).

Antidunes in rivers often occur in trains of width less than the flow width B; their signature is a train of waviness on the water surface. Several trains of surface waves are visible in Fig. 5A, which show flow in the tailings basin of the Hibbing Taconite Mine. In this particular case, the flow was verifiably highly turbulent ($Re \sim 1 \times 10^6$) and Froude supercritical. Similar trains of surface waves were observed in the experiments of Armstrong (2003), as illustrated in Fig. 5B; these are likely candidates for antidunes formed in laminar flow. Indeed, the flow parameters were $H \sim$ 0·8 mm and $U \sim$ 0·42 m sec^{-1}. The Reynolds number Re was near $\sim$ 360 and the Froude number was highly supercritical, with $Fr \sim$ 4·6.

Coleman *et al.* (1998) also noted the occurrence of antidunes for five of their tests of laminar open-channel flows. These experiments were for ν = 1 × 10^{-4} m^2 sec^{-1}, D = 0·28 to 1·57 mm, R = 1·65, H = 0·034 to 0·058 m, U = 0·428 to 1·256 m sec^{-1}, Fr = 0·57 to 2·17, Re = 248 to 427 (laminar flow), and τ^* = 1·7 to 6·9 (from which it can be inferred that sediment was in motion). Owing to a lack of sediment supply, a scour hole formed at the upstream end of the erodible-bed section for each of these experiments. The flow responded to the scour-hole profile by generating a train of in-phase antidunes.

Single-row and multiple-row bars in laminar flow

Bars form in rivers when the ratio B/H of width to depth is sufficiently high. These bars may form as single-row alternate bars, as shown in Fig. 6A for the case of the Naka River, Japan, or as multiple-row linguoid bars, as shown in Fig. 6B for the case of the Fuefuki River, Japan.

Armstrong (2003) observed the formation of both single-row and multiple-row bars in laminar flow; the former are shown in Fig. 6C (compare with the field case of Fig. 6A) and the latter in Fig. 6D (compare with the field case of Fig. 6B). In the case of these experiments the flow parameters were as follows: $H \sim$ 1·2 mm, $U \sim$ 0·17 m sec^{-1}, $Re \sim$ 208 and $Fr \sim$ 1·5.

Self-formed meandering channels in nearly laminar and laminar flow

Figure 7A shows a view of the meandering Chinchaga River in Alberta, Canada. While a simulation of the onset of channel meandering in the laboratory is relatively easy (e.g. Parker, 1976), until recently no researcher has succeeded in developing self-formed, high-amplitude meandering channels in the laboratory.

Smith (1998), however, was able to develop self-formed laboratory meanders that became so sinuous that some bends were subject to cut-off, as illustrated in Fig. 7B. Two of the materials used by Smith were a mixture of diatomaceous earth and calcined white China clay. The chan-

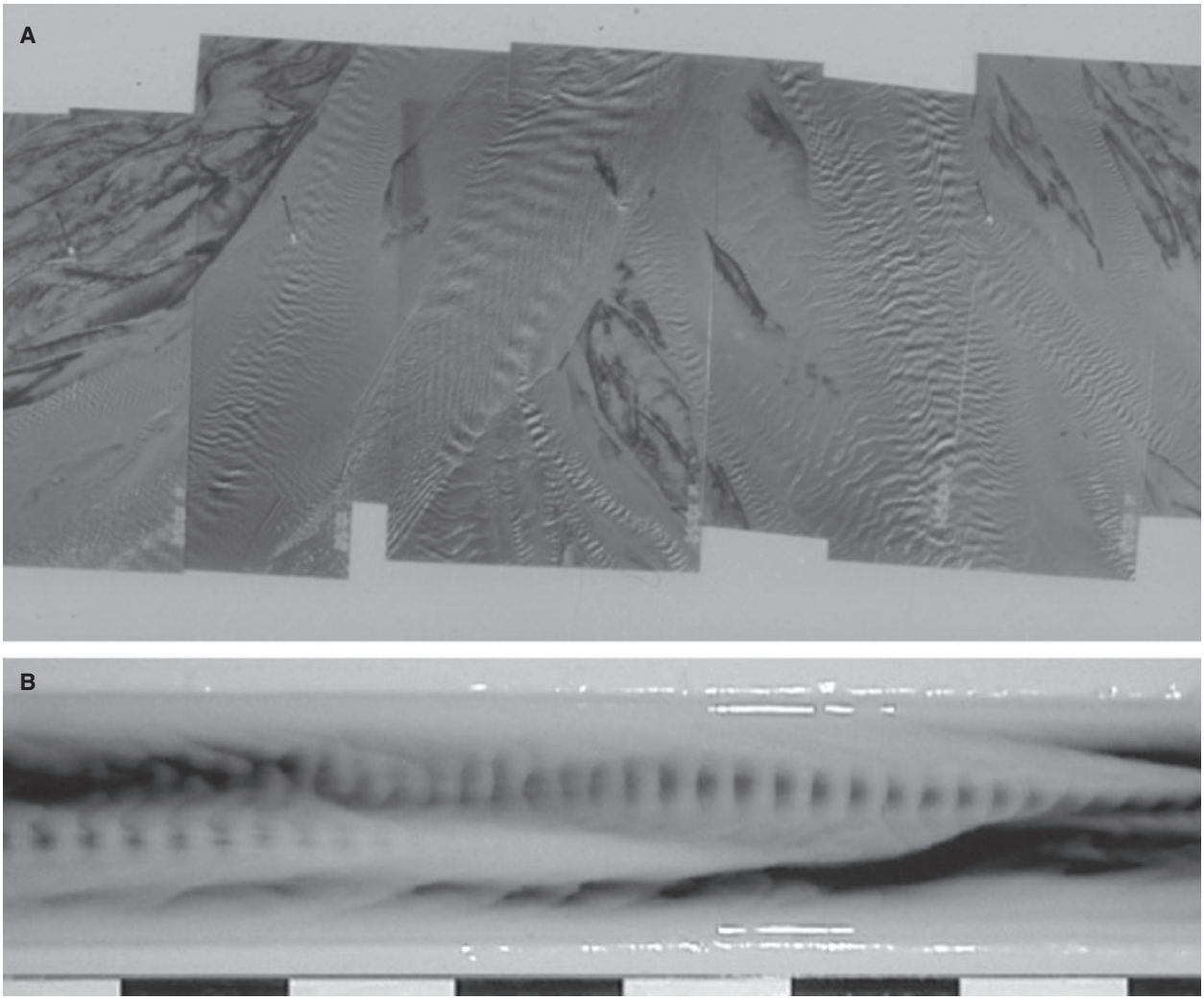

Fig. 5. (A) Aerial view of flow in the tailings basin of the Hibbing Taconite Mine in Minnesota, USA. Flow is from top to bottom. The trains of surface waves are the signature of antidunes. The wavelength of the surface waves varies between 0·5 m and 1·0 m. (B) Wave trains in one of the experiments of Armstrong (2003) that suggest the presence of antidunes. The flow is from right to left and the scale is in centimetres.

nels actively migrated and constructed point bars. Values of *Re* for the flow were estimated to range from about 750 to about 1000. Thus, although the flow was not strictly laminar, the turbulence can be expected to have been poorly developed, as indicated by Eq. 4b.

The conditions that were seen to be important for the formation of meanders at model scale were readily identifiable. Of critical importance was the use of easily transported, fine-grained sediments with slight cohesion. The small grain size of the sediment, of the order of 4 to 30 μm, enabled point-bar deposits to form readily in the microscale river developed by Smith, where the flow depth varied typically between 5 and 7 mm. Cohesion encouraged the formation of well-defined, single-thread channels. Cohesion also allowed point bars to consolidate over time so as to be resistant to subsequent erosion. The instabilities that led to meanders were seen to be the result of sufficient longitudinal slope and an adequate sediment supply. Formative bed slopes ranged from 0·007 to 0·02 and formative flow discharges ranged from 10 to 40 ml sec^{-1}.

The above description strongly suggests that the essential element for high-amplitude meander formation in the experiments of Smith (1998) was the mild cohesivity of the sediment, and not the existence or absence of turbulence; this notwithstanding, the flow conditions were not in the range of purely laminar flow. This issue was addressed here by studying experimentally the stability of an initially straight channel under conditions of purely laminar flow. The present

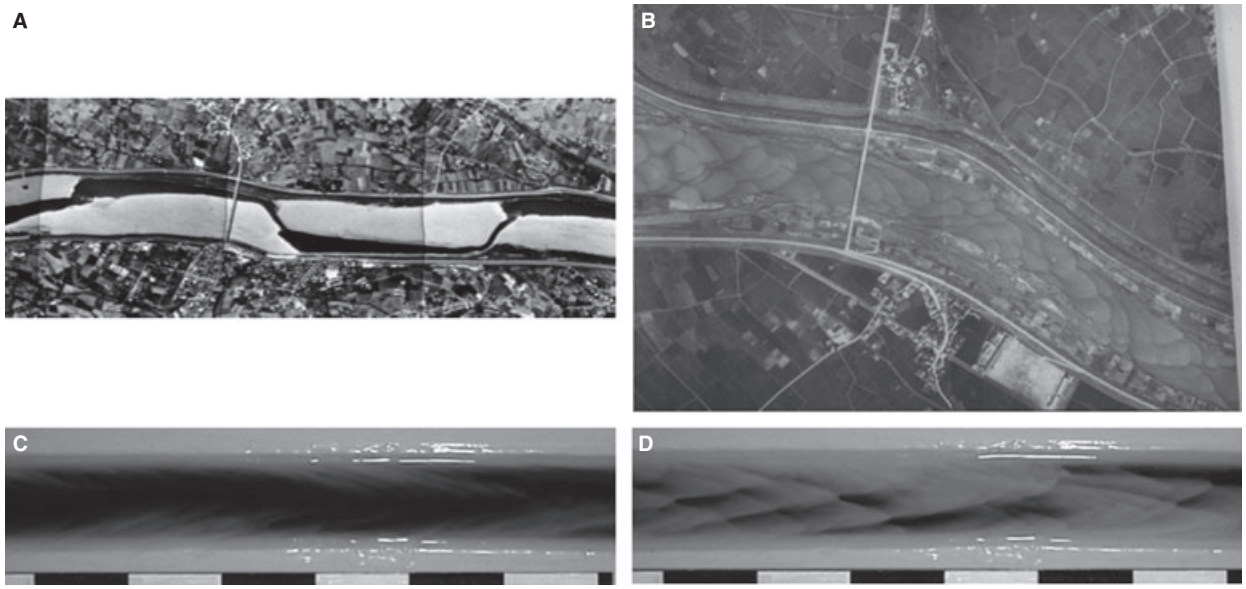

Fig. 6. (A) Single-row alternate bars in the Naka River, Japan at low flow. The image is courtesy of S. Ikeda. (B) Multiple row linguoid bars in the Fuefuki River, Japan. The image is courtesy of S. Ikeda. (C) Single-row alternate bars and (D) multiple-row linguoid bars observed in experiments from Armstrong (2003). The flow was laminar in both cases. Flow direction is from left to right in all diagrams. The scale for (C) and (D) is in centimetres.

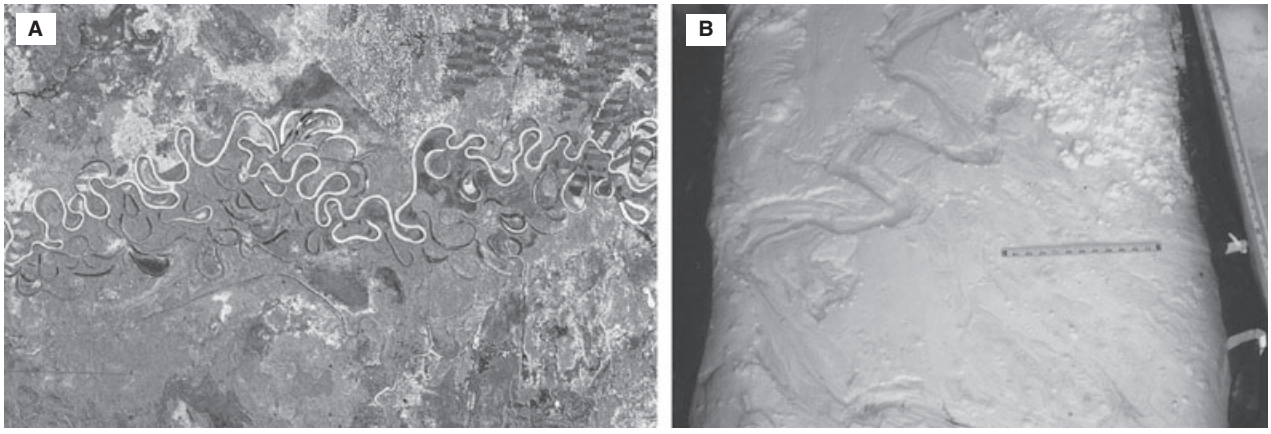

Fig. 7. (A) The meandering Chinchaga River, Canada. Flow is from left to right. The image is from the NASA MrSID website. The width of the imaged zone is *ca* 20 m. (B) Self-formed high-amplitude meanders formed in the laboratory under nearly laminar flow conditions. Flow is from top to bottom. From Smith (1998).

experiments were similar to those of Armstrong (2003), except for the sediment grain size which varied in the range 400 to 600 μm and was therefore much coarser than the 50 to 100 μm sediment used by Armstrong (2003). A more detailed description of the experimental protocol can be found in Meunier & Métivier (2000) and Métivier & Meunier (2003). Each experiment was commenced by carving a straight channel into the sediment bed. Under the action of the flow, this initially straight channel rapidly evolved into a mildly sinuous channel with well-developed point bars. An example for which $Re = 84$ and $Fr = 3{\cdot}48$ is shown in Fig. 8. In this experiment, a laser line was used to measure the topography and the flow depth along the channel section. Figure 8 shows the channel with [panel (A)] and without [panel (B)] flow, together with the laser line, the computed water depth and hydraulic parameters [panel (C)]. The depth of flow was computed from the differences in position of the two laser lines that are caused by refraction of light in water. This technique yielded flow depths of the order of a millimetre. The corresponding flow velocities were estimated from the knowledge of flow depth and water flow rate using

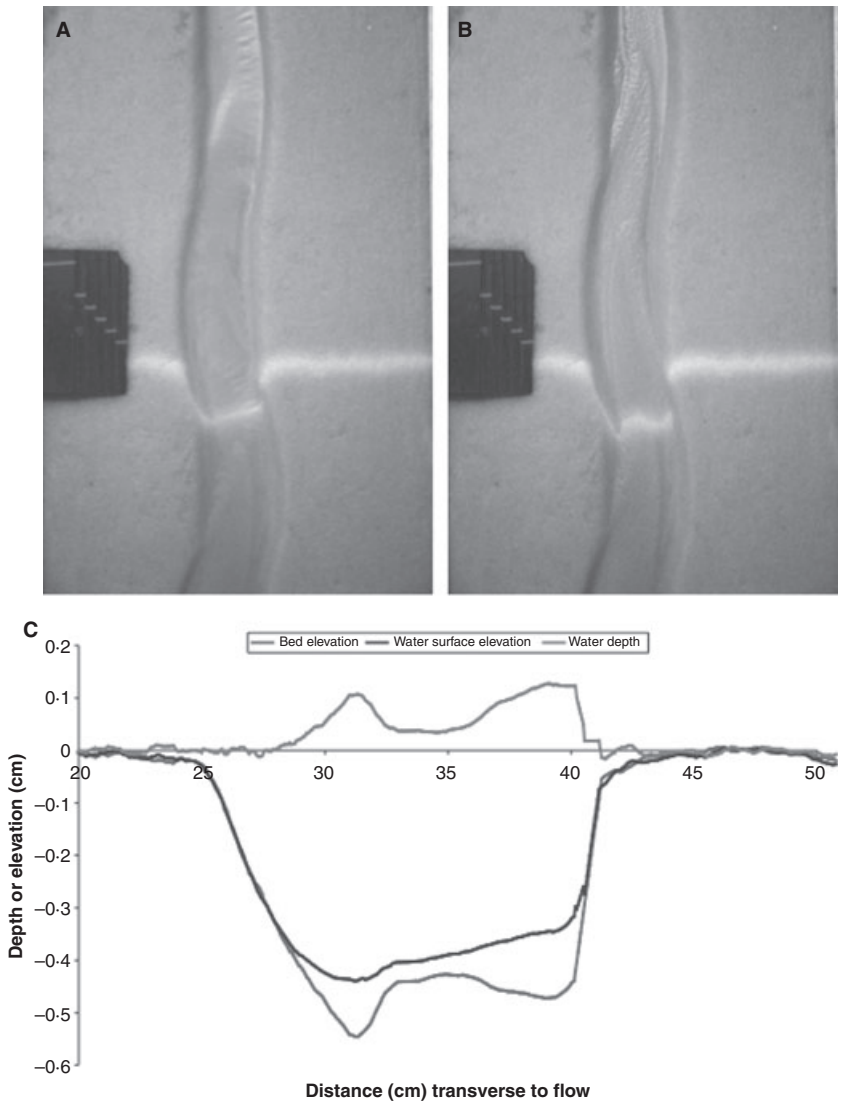

Fig. 8. Two images of a laminar sinuous channel with point bar: (A) image with flow; and (B) image without flow. The laser line used to reproduce both topography and flow depth is in white. The reference scale used to calibrate the topography measurements is visible on the left-hand side of the images. (C) Transverse elevation profiles of the sediment bed (dashed light grey) and the water surface (dashed dark grey). The water flow depth is also plotted (continuous black line).

mass conservation; they ranged from 0·1 to 0·5 m sec^{-1}. The results also unambiguously show that the flows so observed were laminar.

As coarse glass beads (400 to 600 μm) were used, the cohesive properties of importance in the investigation by Smith were absent in the present experiments. As a result, and given enough time, the channels invariably evolved into a braided configuration. This effect was not a consequence of the flow being laminar rather than turbulent. When analogous experiments are performed under conditions of turbulent flow, an initial channel showing mild meandering also eventually evolves into a braided configuration (e.g. fig. 4 of Federici & Paola, 2003). The reason for this evolution is the lack of any kind of bank cohesion (cohesive sediment or vegetation), not turbulence or the lack of it (Tal & Paola, 2007).

Braiding in laminar flow

Figure 9A shows an aerial view of part of the Skeithara Sandur in Iceland. The Skeithara Sandur, which emanates from the Vatnajokull glacier, is one of the largest braided rivers in the world. One of the earliest contributions to the study of rivers using laminar-flow microscale models is that of Hong & Davies (1979). These authors showed that braiding was a stable state for a steady laminar-flow self-formed stream flowing over fine sand in a sand tray 5 m long and 1 m wide. Persistent braiding was achieved both by allowing the stream to widen from an initial narrower channel, and also by allowing braiding to develop from an initially broad, completely plane bed covered by a uniform shallow sheet flow. In this work, the sediment was rounded silica sand with $D_{50} = 0{\cdot}19$ mm and the flow depth H was

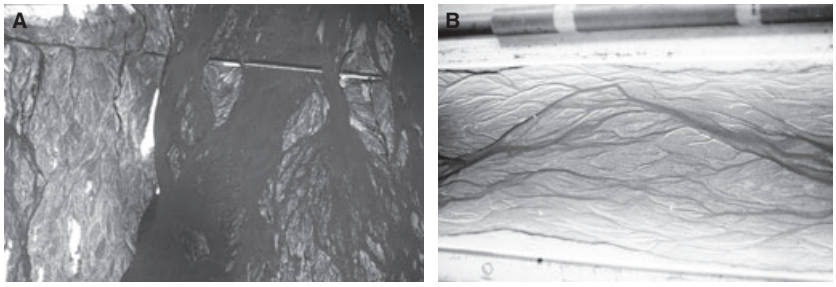

Fig. 9. (A) The braided Skeithara Sandur of Iceland, shortly after the jökulhlaup flood of 1996. The damaged bridge provides some indication of scale. Flow is from top to bottom. The image is courtesy of H. Johannesson. (B) A braided river formed in the laboratory under conditions of laminar flow. The flow has been turned off for clarity. The experimental flume is 1 m wide and 5 m long. Flow is from left to right. From the experiments of Hong & Davies (1979).

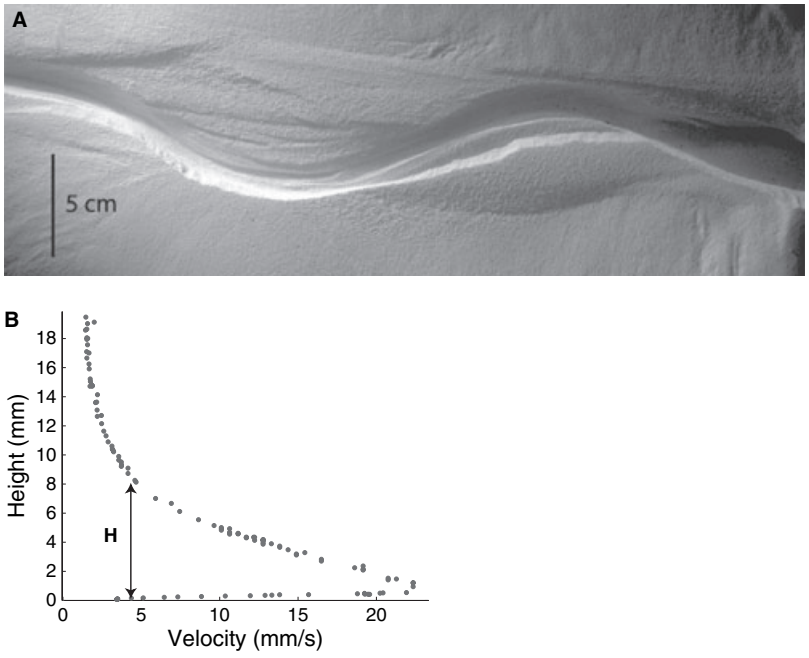

Fig. 10. (A) Meandering submarine canyon formed in one of the experiments of Métivier *et al.* (2005). Flow is from right to left. (B) Velocity profile inside the experimental density current measured using the Particle Shadow Tracking method (Lancien *et al.*, 2007). The characteristic flow depth 'H' of the density current is shown on the plot.

$\sim$1 mm with a velocity of $\sim$100 mm sec^{-1}, giving a maximum Reynolds number of $\sim$100. Figure 9B shows the braiding pattern that developed.

A more recent study (Davies *et al.*, 2003), with very similar parameters showed that a steady-flow laminar model was capable of representing rather accurately the spatial distribution of relative erosion and deposition measured in the braided bedload-dominated Waiho River, New Zealand. The model did not satisfy Reynolds similarity with the prototype, with $Re \sim 300$ in the model but $\sim 2 \times 10^6$ in the prototype. In addition, the mean bed slope of the model was about eight times that of the prototype. Froude similarity was, however, satisfied, with $Fr = 0{\cdot}7$ in both cases. A detailed comparison of laboratory and prototype parameters is given in Table 1. The authors note the following with regard to the patterns of aggradation and degradation. ''[Model] behaviour corresponds extremely well with data from bed-level surveys between 1985 and 1993… The spatial pattern of aggradation is strikingly similar in both cases…''.

Reynolds numbers in both the models of Hong & Davies (1979) and Davies *et al.* (2003) were much less than about 500, so that flow was always laminar, whereas those in the Waiho River greatly exceed this value, as noted above. The detailed processes of water flow and sediment motion are therefore likely to differ from those in field-scale rivers. This difference does not prevent channel pattern variability in the model from being similar to that in the prototype. Hong & Davies (1979), for example, found that the number of braids in a microscale model braided river was similar to that in the 1 km wide prototype Rakaia River,

New Zealand. This finding, and the success of the Waiho model, suggest that the spatial distribution of relative erosion and deposition was, in both cases, controlled by the planform geometry of the river, since this, relative depth and Froude number were the only parameters with similarity between model and prototype. Similar success with very small-scale mobile-bed models has been reported by Gaines & Mainord (2001).

Sinuous subaqueous canyons excavated by laminar dense underflows: levéed channels emplaced by laminar or near-laminar turbidity currents

The submarine world has analogues to fluvial morphologies, including bedforms, meandering channels, canyons and fans. These morphologies are created by turbidity currents, which are submarine analogues of river flows. Microscale experiments performed using laminar flow have proved useful in the study of these flows as well. Turbidity currents are characterized by high suspended sediment concentrations which drive the flow. As noted above, rectilinear laminar flows are not capable of entraining sediment into suspension; this notwithstanding, a turbidity current can be modelled using a dense saline underflow, with the resulting morphodynamics driven by bedload transport. Alternatively, a laminar turbidity current can be driven by fine sediment that has been suspended by a separate mechanism, and which is then allowed to settle out slowly as the flow progresses downstream.

Métivier *et al.* (2005) have modelled the formation of sinuous submarine canyons at microscale. The flow was a bottom current driven by dissolved salt, which was allowed to rework an erodible bed via differential bedload transport. The experimental set-up consisted of a 100×50 cm inclined plane immersed in a $200 \times 50 \times 50$ cm plastic tank filled with fresh water. Sediment particles (a plastic powder with a solid density of $\rho_s = 1080$ kg m^{-3} and a median grain size of 27 μm) were put into suspension in the fresh water of the tank and allowed to settle randomly. This process led to the deposition on the inclined plane of an erodible bed of initial thickness of the order of a few centimetres. Once the plastic powder had completely settled, a brine of adjustable density ρ_f was injected at a constant flow discharge Q from the top of the incline. As a result, a bottom density current developed along the incline. Depending on the values of the slope of the bed (which varied in the range 10° to 20°) and those of Q (which varied between 0·06 and 0·6 l min^{-1}), erosion and deposition of the bed particles could occur and lead to the formation of an incisional channel. The formation of this channel was accompanied by a depositional lobe immediately downstream that prograded as incision propagated downstream.

Such an incisional channel is shown in Fig. 10A. The formation of both meanders and terraces was observed. A method called 'particle shadow tracking' (Lancien *et al.*, 2007) was developed in order to measure the velocity profile of the density current. The resulting data were used to estimate the average velocity and the characteristic flow depth of the density current as shown in Fig. 10B. The calculated Shields and Reynolds numbers fell in the range $\tau^* \sim 0{\cdot}6$ to 1·5 and $Re \sim 100$ to 300 (Lancien, 2007), thus demonstrating the possibility of reproducing submarine channels in a laminar microscale experiment.

Turbidity currents on submarine fans and submarine fairways often channellize themselves between high levées (e.g. Pirmez & Flood, 1995). Recently, Yu *et al.* (2006) succeeded in modelling self-formed levéed channels at a small-scale in the laboratory. The experiments were conducted in a 3·9 m long, 2·15 m wide and 0·6 m deep rectangular basin at St Anthony Falls Laboratory, University of Minnesota. The basin was filled to a depth of 0·57 m with tap water. A platform located in the basin with a slope of 7% was used to provide a base slope for the turbidity currents. A mixing tank with a volume of 189 l placed above the upstream end of the basin was used to introduce turbid water. Inflow discharge was set with a range varying between 0·015 and 0·05 l sec^{-1} depending on the experiment.

In each experiment, a slurry with a concentration of 10% by volume was introduced near the upstream end of the tank. The sediment was composed of equal portions of four sediment types: (i) 110 μm silica flour; (ii) 45 μm silica flour; (iii) 20 μm silica flour; and (iv) kaolinite clay. The water–sediment mixture was introduced from the mixing tank into the main tank via a flexible pipe at a point at the transverse centre of the basin and 15 to 20 cm downstream of the upstream wall. Deposition of nearly all of the coarser fractions of sediment near the outfall of the pipe led to the formation of a cone-shaped fan topped by a crater-like structure just below the outfall point. This deposition was accompanied by copious entrainment of ambient water, causing dilution of the fine-grained turbidity current. The flow spread radially down the cone,

Fig. 11. View of levéed channels emplaced by a laminar or near-laminar turbidity current in the laboratory. Flow is from top to bottom. The width of the experimental flume is 2·15 m.

and then down the platform, in the form of a sheet-like turbidity current. Although the interface between the turbidity current and the ambient water was turbulent on the cone, this turbulence quickly died out as the flow progressed to the platform itself. The thin turbidity current evidently was unstable, as it tended to concentrate to form long, levéed channels that were much narrower than the tank itself. Typical channels so formed are illustrated in Fig. 11.

The channels tended to have widths between 15 and 30 cm and depths between 0·1 and 0·2 cm. The characteristic thickness of the flow over the channel was estimated as ~1 cm, and the characteristic flow velocity was estimated as ~5 cm sec^{-1}. Assuming that the sediment-laden flow was sufficiently dilute to have the same viscosity as water at 20 °C, flow Reynolds numbers could be estimated as ~500, implying laminar flow.

The 3D configuration of these very thin flows did not allow for sampling of the water–sediment mixture to determine sediment concentration. For this reason, Johnson *et al.* (2008) reproduced the same range of flow conditions in a much narrower flume with a width of 10 cm. Samples of suspended sediment were taken and, in addition, more detailed measurements of flow velocity and thickness were made. The data analysis therein provides strong confirmatory evidence that the flows of Yu *et al.* (2006), which emplaced levéed channels, were laminar and driven by dilute suspensions of kaolinite clay.

Turbidity currents, then, need not be turbulent; although they are driven by the excess weight of suspended sediment, the current can be sustained for some distance in the absence of turbulent resuspension, as long as the fall velocity of the sediment is sufficiently small. In the laminar flow region of the experiments of Yu *et al.* (2006), the kaolinite was maintained in the water column simply because the fall velocity was so small that not all of the sediment could deposit before reaching the end of the experimental platform. Yu *et al.* (2006) argue that the levées observed in their experiments probably were emplaced by means of inhibited deposition near the channel centre, even in the absence of turbulence and turbulent entrainment of sediment.

TEA LEAVES AND CHANNEL BENDS: FLOWS WITH THE SAME UNDERLYING PHYSICS NEED NOT BE DYNAMICALLY SIMILAR

Einstein (1926) endeavoured to understand the morphodynamics of meandering rivers by observing tea leaves in a stirred cup: ''Imagine a flat-bottomed cup full of tea. At the bottom there are some tea leaves, which stay there because they are rather heavier than the liquid they have replaced. If the liquid is made to rotate by a spoon, the leaves will soon collect in the centre of the bottom of the cup''. Einstein used this example to infer the existence of a near-bed secondary flow in a river bend that drives sediment toward the inner bank. The existence of this flow pattern at field scale was documented earlier by Thompson (1876) and was later explained in terms of fluid mechanics by, for example, Rozovskii (1961).

River flow is invariably turbulent. It is possible to make the flow created by stirring the teacup laminar by reducing the size of the cup or the speed of stirring, or by adding honey to the tea; and yet both flows illustrate the same phenomenon, i.e. the tendency for heavy detritus to be moved radially inward along the bed. Is this coincidence, or is there something more to the analogy?

Two flows are said to be dynamically similar if all the dimensionless ratios that can be formed using the relevant physical parameters of the problem have the same values for both flows. Thus, the flow of water ($\nu = 1 \times 10^{-6}$ m^2 sec^{-1}) in a pipe with a diameter D of 0·001 m at a speed U of 0·1 m sec^{-1} is dynamically similar to the flow of a glycerine–water mixture ($\nu = 1 \times 10^{-4}$ m^2 sec^{-1}) in a pipe with a diameter D of 0·05 m at a speed of 0·2 m sec^{-1}, to the extent that the Reynolds number Re_p is 200 in both cases. A flow in a teacup with a Reynolds number of the order of 10^2 cannot possibly satisfy Reynolds similarity with the flow in the bend of, for example, the Mississippi River, for which the Reynolds number is of the order of 10^7. Can teacups then be used to infer river morphodynamics?

The answer is affirmative. When dynamical similarity is rigorously satisfied, the physics of the two flows are identical. However, even when dynamical similarity is not satisfied, it is possible for a pair of flows to be simply two different manifestations of the same phenomenon, both of which are described by a shared physical framework. Any given analogy must not be overplayed because the lack of complete dynamic similarity implies that different features of a phenomenon may be manifested with different relative strengths. This shared framework nevertheless allows laminar-flow morphodynamics to shed useful light on turbulent-flow analogues.

A more specific example is used in the following to illustrate the above point. Secondary flow in river bends has long been known to play an important (but by no means the sole) role in the establishment of point-bar morphology (e.g. Engelund, 1974). Although bend secondary flow has been described in various papers, a brief summary of the model of Engelund (1974) serves to illustrate this point. The flow can be most easily understood in terms of flow in a wide, spiral open channel with constant centreline radius of curvature R_c (Fig. 12). Let z denote upward-normal distance from the bed, and let $u_s(z)$ denote the vertical profile of streamwise (primary) flow velocity. The outward-directed centrifugal force per unit mass experienced by the flow particles as they traverse the bend is u_{sc}/R_c. This centrifugal force is balanced by super-elevating the flow, so that the free surface toward the outside of the bed is higher than that toward the inside of the bend. This effect generates an inward-directed deviatoric pressure force per unit mass with the magnitude gS_{tw}, where g denotes gravitational acceleration and S_{tw} denotes the magnitude of the transverse water surface slope (Fig. 12).

The balance between centrifugal and deviatoric pressure forces, however, cannot be perfect because the deviatoric pressure force is constant in the vertical, whereas the centrifugal force is proportional to u_s^2 and u_s varies in z. The result, as shown in Fig. 12, is a cell of secondary flow that is directed from outer bank to inner bank near the bed, and in the opposite direction near the water surface.

Nothing about the above picture requires the flow to be turbulent. All that is required is a profile of primary flow velocity $u_s(z)$ such that u increases monotonically in z. Indeed, Rozovskii (1961) solved for the secondary flow in a bend in

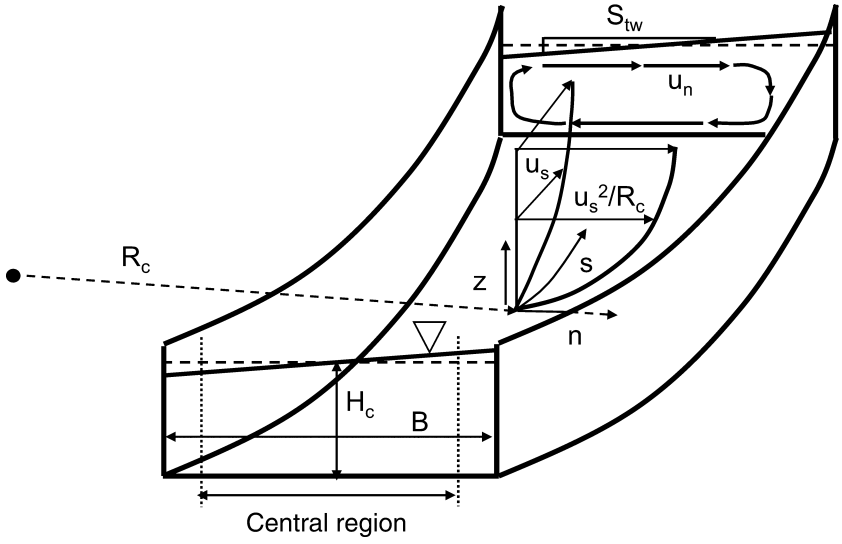

Fig. 12. Definition diagram for steady, streamwise-uniform open channel flow in a bend of constant curvature.

Table 1. Comparison of laminar and turbulent flow values of various parameters for two cases of bend flow.

	Turbulent	Laminar
B (m)	40	0·02
H_c (m)	3	0·0015
R_c (m)	200	0·1
U (m sec^{-1})	2	0·1
B/H_c	13·3	13·3
H_c/R_c	0·015	0·015
C_z	11·66	7·17
Re	$6{\cdot}00 \times 10^6$	150
Fr	0·369	0·824
S	0·001	0·0136
G_s	0·0338	0·0536
u_{ns}/U	0·0768	0·121

the case of turbulent flow (logarithmic profile of primary velocity) and Yen (1972) obtained the corresponding solution for a laminar flow (parabolic profile of primary velocity).

The issue in question is examined in more detail in the *Appendix* using the formulation of Engelund (1974). It suffices to note here that governing equation and boundary conditions for the secondary flow can be reduced to dimensionless forms encompassing both laminar and turbulent flow, and from which the laminar case is obtained by setting a single dimensionless parameter equal to zero. The conversion to a dimensioned form for the cross-stream velocity u_s involves a term that depends on the Reynolds number for laminar flow, but that is independent of the Reynolds number for turbulent flow in the hydraulically rough regime; and yet the basic structure is so similar that it indicates that aspects of the morphodynamics of meandering rivers can be reproduced and studied at the scale of laminar or nearly laminar flows. In order to illustrate this idea, two flows in channel bends, one being laminar microscale and the other being turbulent field scale, are compared quantitatively in the *Appendix*. Table 1 illustrates the results of this analysis.

The parameters in the Table that have not previously been defined are channel centreline depth H_c, depth-averaged streamwise flow velocity U, bed slope S and near-surface velocity of secondary flow u_{ns}. Two more parameters, the dimensionless friction coefficient C_z and an appropriately scaled dimensionless near-surface value of the secondary flow G_s, are defined in the *Appendix*. The turbulent field-scale case in the Table is based on the estimates of parameters that fall within the range of gravel-bed rivers studied by Parker *et al.* (2007). The values for the microscale case are in the same range as those presented in Fig. 8.

The parameters have been chosen so as to satisfy similarity between microscale and field scale in the parameters B/R_c and H_c/B. Note that the field-scale Reynolds number is 40 000 times larger than that applying to the microscale value. The microscale slope is 14 times larger than the field-scale value, and the microscale Froude number is 2·2 times larger. The two flows thus are not dynamically similar in the general sense; this notwithstanding, the Chezy coefficient C_z, and the surface values pertaining to the secondary flow G_s and u_{ns}/U are all of the same order of magnitude. More specifically, the ratios of the laminar value to the corresponding turbulent value for all three of the parameters C_z, G_s and u_{ns}/U fall between 0·5 and 2·0. As long as the bed is mobile in both cases, similarity in the friction coefficient and secondary flow is sufficient to ensure an analogous fluid-mechanical driver for point-bar morphodynamics.

A RECIPE FOR TRANSLATING TURBULENT MORPHODYNAMICS TO LAMINAR MORPHODYNAMICS IN TERMS OF ANALOGOUS PHYSICS

Fluid mechanics of steady, streamwise-uniform flow in wide open channels: laminar versus turbulent flow

Laminar and turbulent open-channel flows are different, and yet their underlying structure contains essential analogies which are explored here. For the sake of clarity, this section contains some overlap with the material presented in the *Appendix*.

Consider the case of steady, streamwise-uniform (normal) flow in a wide open channel of constant bed slope S and depth H. Let z denote an upward-normal (quasi-vertical) coordinate, $u(z)$ denote the local streamwise flow velocity at elevation z and U denote the depth-averaged value of u. The relevant relation for laminar flow is a parabolic law, i.e.:

$$\frac{u}{U} = 3\left(\zeta - \frac{1}{2}\zeta^2\right) \tag{17}$$

where in analogy to Eq. A5b:

$$\zeta = \frac{z}{H} \tag{18}$$

Defining the bed resistance coefficient C_f according to Eq. A7, the relevant resistance relation for laminar flow is:

$$C_f = \frac{3}{Re} \tag{19}$$

In the case of turbulent flow over a rough bed with equivalent roughness height k_c (here taken to be a composite value including the effects of grain roughness and bedforms), the velocity profile is most commonly represented in terms of a logarithmic or power formulation. In order to emphasize the analogy with laminar flow, however, it is more illustrative to use the equivalent slip velocity formulation of Engelund (1974) presented in the *Appendix*. Thus:

$$\frac{u}{U} = \frac{\chi + \zeta - (1/2)\zeta^2}{\chi_1}, \quad \chi = \chi_1 - \frac{1}{3} \tag{20a,b}$$

where:

$$\chi_1 = \frac{1}{13} C_f^{-1/2} \tag{21}$$

and C_f satisfies the Keulegan (1938) relation for rough turbulent flow:

$$C_f^{-1/2} = 6 + 2 \cdot 5 \ln\left(\frac{H}{k_c}\right) \tag{22}$$

Now laminar and turbulent flows satisfy very different resistance relations that do not scale with each other, i.e. Eq. 19 versus Eq. 22; and yet the dimensionless velocity profiles given by Eqs 17 and 20a,b are analogous to the point that Eq. 20a,b converges to Eq. 17 in the limit as $\chi \to 0$. This similarity in velocity profiles is the result of a similarity of physical processes: Both molecular and turbulent processes act to diffuse flow quantities, including stream flow momentum, from zones of high concentration (near the water surface) to zones of low concentration (near the bed). The result is velocity profiles that show analogous tendencies for velocity to increase toward the water surface.

The above relations provide a recipe for converting theories and formulations of turbulent-flow morphodynamics into those for laminar-flow morphodynamics. That is one has to retain the overall structure of the formulation, but simply replace relations of the type of Eqs 20a,b and 22 of turbulent flow to corresponding relations of the type of Eqs 17 and 19 for laminar flow.

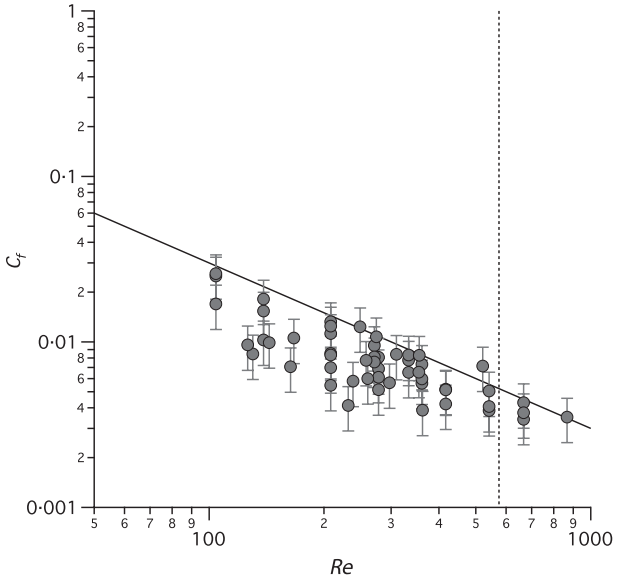

Fig. 13. Plot of C_f versus Reynolds number *Re*. Circles correspond to data from Armstrong (2003), the straight line corresponds to the theoretical line of Eq. 19 and the dashed line corresponds to the criterion *Re* = 575 below which laminar flow prevails.

The self-formed laminar channels of Armstrong (2003)

Before continuing, three features of the self-formed open channels of Armstrong (2003) that were introduced earlier are demonstrated: (i) the flows are indeed laminar; and they are unaffected by: (ii) bank friction; and (iii) surface tension.

The experimental flows of Armstrong (2003) were sufficiently thin so as to make measurements of velocity profiles impossible. It is, however, possible to test the friction relation, Eq. 19. Figure 13 shows a plot of C_f calculated from Eq. A7 versus *Re* for the channels of Armstrong (2003). The data follow the trend of Eq. 19, but the friction coefficients inferred from the data are generally lower than the predicted values by an average multiplicative factor of 0·707. The most likely reason for this is the uncertainty in the velocity measurements. If it is assumed that the mean velocity of the flow is 0·9 times the value measured from video records of surface dye tracer motion, the data fit the theoretical relation quite well. It is reasonable, then, to assume that these flows are laminar.

The channels are sufficiently wide so that bank effects do not substantially affect the resistance relation; this is shown in Fig. 14, in which the parameter $C_f \times Re/3$ (which should be unity according to Eq. 19) is plotted against aspect ratio B/H, where B denotes channel width. While the values of $C_f \times Re/3$ fall below unity, as in Fig. 13, no significant trend in aspect ratio is seen.

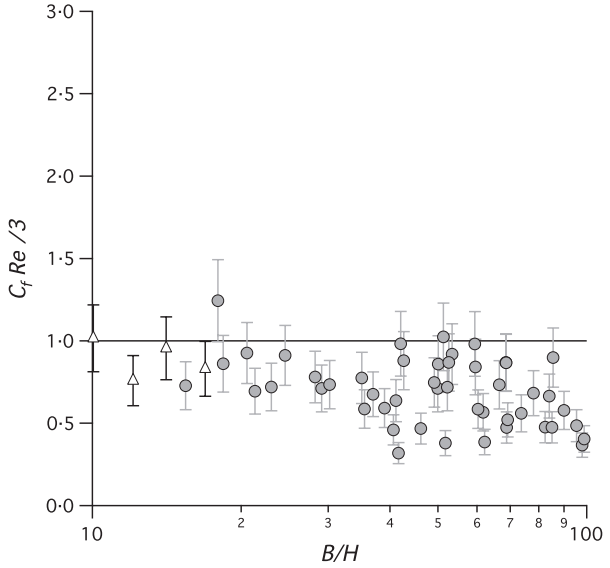

Fig. 14. Plot of $C_f \times Re/3$ versus aspect ratio B/H. Included are data from Armstrong (2003) and the theoretical line of Eq. 19. Circles and triangles correspond, respectively, to flows that are fully laminar flows ($Re \leq 575$) or transitional to full turbulence flows ($575 \leq Re < 1000$), respectively.

Indeed, $C_f \times Re/3$ approaches unity most closely for the narrowest channels.

It might be argued that surface tension has an effect on these micro-channels (Peakall & Warburton, 1996; Malverti *et al.*, 2008). To test this, $C_f \times Re/3$ versus two dimensionless measures of surface tension were plotted: a channel Bond number $\mathrm{Bo_c}$ and a channel Weber number We_c, defined, respectively, as:

$$\mathrm{Bo_c} = \frac{\rho g B^2}{\sigma}, \quad We_c = \frac{\rho U^2 H}{\sigma} \qquad (23a,b)$$

where σ denotes surface tension. The relevant plots are given in Fig. 15A and B. No effect of surface tension is discernible in either plot, no matter whether the flow is fully laminar ($Re \leq 575$) or transitional to full turbulence ($575 \leq Re < 1000$).

Examples of translations and potential translations of existing formulations

The analogous nature of the underlying physics allows the potential for a direct translation of many theories of turbulent morphodynamics to laminar flow. The theories in question include self-formed channels, dunes and antidunes, single-row and multiple-row bars, meandering and braiding.

The first case to be described here is one in which the translation has been achieved. Many stability theories have been developed to describe the formation of single-row and alternate-row bars in rivers. Two prominent examples include Kuroki & Kishi (1984) and Blondeaux & Seminara (1985). These treatments use a two-dimensional shallow water formulation for the flow with: (i) a resistance relation for turbulent flow; (ii) a correction for curvature-induced secondary

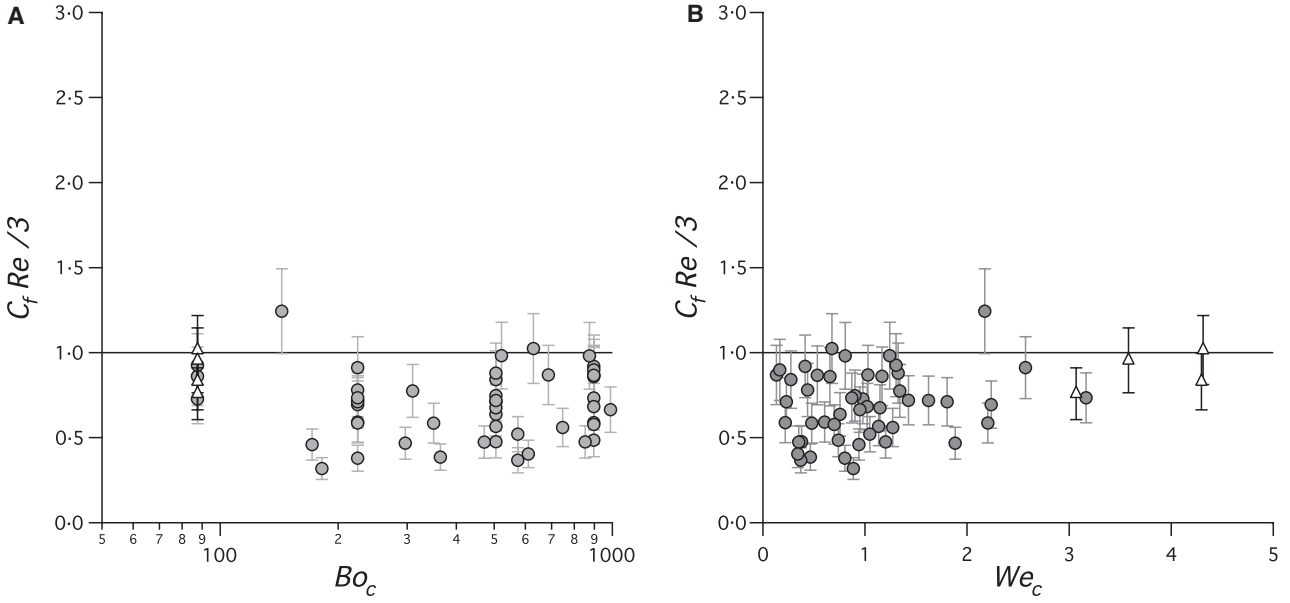

Fig. 15. Plot of $C_f \times Re/3$ versus (A) channel Bond number $\mathrm{Bo_c}$ and (B) channel Weber number We_c. Included are data from Armstrong (2003) and the theoretical line of Eq. 19. Circles and triangles correspond to flows that are fully laminar flows ($Re \leq 575$) or transitional to full turbulence flows ($575 \leq Re < 1000$), respectively.

flow based on analysis of the type presented in the *Appendix*; and (iii) a 2D generalization of a sediment transport equation such as Eq. 10a,b. It is of interest to note that such analyses of alternate bars show no singularity or abrupt change in behaviour as the flow passes from subcritical to supercritical. Alternate bars can and do form for either case.

The translation to laminar flow is straightforward: (i) replace the flow resistance relation with a laminar one, i.e. Eq. 19; (ii) replace the secondary flow correction with a laminar one of the type presented in the *Appendix*; and (iii) replace the sediment transport relation with a form for laminar flow such as Eq. 15a,b (the 2D generalization of which is straightforward, based on the formulation given in Garcia, 2008). Such an analysis has already been carried out successfully by Devauchelle *et al.* (2007); the results show that the major bar structures characteristic of natural rivers are qualitatively retrieved in a laminar flow.

Parker (1978) has developed a theory describing how a mobile bed can coexist with a stable width and stable banks in the case of bedload-dominated channels. The key feature in the analysis is a description of the transverse transport of streamwise momentum by turbulent diffusion. A simple translation from turbulent diffusion to laminar diffusion offers a recipe for explaining the self-formed channels of Armstrong (2003).

There is a long history of theoretical analysis that uses the fluid mechanics of flow over wavy beds to explain the origin of dunes and antidunes. The original potential flow analyses due to Anderson (1953) and Kennedy (1963) apply as a first approximation to both laminar and turbulent flow over dunes and antidunes, as long as the Reynolds number is sufficiently high (e.g. $Re > \sim 50$) and provided that the length scale considered is short compared with that associated with frictional dissipation of flow energy. Smith (1970), Engelund (1970) and Fredsøe (1974) generalized these potential flow analyses to frictional, turbulent shear flow, so obtaining stability theories describing the origins of dunes and/or antidunes.

In the case of dunes, the translation to laminar flow is best illustrated by the formulation of Smith (1970). Smith simply used a laminar-flow formulation for the velocity profile, but increased the kinematic viscosity ν so as to fall in the range of turbulent flow. The theory, however, predicts a range of dune instability for any value of ν. A formal theory for laminar dunes thus already exists.

While the formulations of Engelund (1970) and Fredsøe (1974) can be similarly adapted to explain dunes under conditions of laminar flow, they associate antidunes in sand-bed streams with sediment suspension. It is known, however, that antidunes can form when bedload transport is the dominant mode of transport as well. The formulation of Parker (1975) for antidunes, which explicitly relies on bedload transport to explain them, is similarly easily adaptable to explain antidunes in laminar flow.

Seminara (2006) has provided a comprehensive survey of recent developments in the theoretical study of the onset, development and maintenance of meandering. Seminara describes meandering as ''…a pattern which offers a fascinating example of the ability that nature often displays to develop highly regular forms…''. The translation to laminar flow is again straightforward, involving the same three steps described above for the case of single-row and multiple-row alternate bars.

Murray & Paola (1994) have used a rule-based cellular model to explain the formation of braided channels. Sun *et al.* (2002) have shown how these 'rules' can be translated into relations that specifically describe sediment transport and flow resistance in turbulent flow. Again, the translation of these rules into those applicable to laminar flow is straightforward.

It should be emphasized that the above discussion offers a recipe for the translation of turbulent-flow morphodynamics into laminar-flow morphodynamics. While the translation has not been specifically carried out for all cases listed, successes with the cases of alternate bars and dunes, combined with the common framework of the physics, offer strong evidence that the translation is possible in general as long as the sediment transport mechanism is bedload transport.

IS TURBULENCE IRRELEVANT?

Based on the discussions above, it would be easy to reach the conclusion that turbulence is irrelevant to erodible-bed morphodynamics. This conclusion would, however, be extreme.

Turbulent-flow morphologies are most likely to have laminar-flow analogues when: (i) the flow is bedload dominated; or (ii) the effect of suspended sediment is felt only through deposition with no resuspension. Even when analogues exist, they must be associated with different transport and resistance relations, and different vertical distri-

butions of flow velocity. As a result the dimensionless scalings for, for example, flow characteristics, geometric characteristics of bedforms and their time development can be expected to differ between the two cases. This difference is illustrated in Table 1, where two bend flows, one laminar and one turbulent, are compared. While the relative strength of the near-surface secondary flow is of the same order of magnitude, the laminar value of u_{ns}/U is larger by a factor of 1·57.

Morphodynamic phenomena in turbulent flow dominated by the differential erosion and deposition of suspended sediment cannot be modelled in laminar flow because laminar flow cannot support equilibrium suspensions. The most common form of antidune in sand-bed rivers, for example, falls into this category (e.g. Engelund & Fredsøe, 1982). In addition, the transition from dunes to upper-regime plane bed is often mediated by the increasing dominance of suspended sediment (e.g. Engelund, 1970). Finally, no mechanism exists for the self-acceleration of turbidity currents in the ocean in the absence of the net entrainment of bed sediment into suspension (e.g. Parker *et al.*, 1986).

CONCLUSIONS

Many fluvial morphologies have been explicitly or implicitly associated with turbulent flow. Indeed, it has been argued that these morphologies are caused by turbulence through the medium of coherent structures. Here it is illustrated that dunes, antidunes, single-row and multiple-row bars, meandering and braiding can be created under conditions of laminar flow. The expressions of these morphologies are notably similar to their analogues for turbulent flow. The similarity does not apply in the sense of dynamic similarity. Rather, it reflects analogous underlying physics. Specific indications are provided herein as to how analytical explanations of these morphologies, based on turbulent flow, can be adapted easily to the case of laminar flow.

This study does not imply that turbulence is irrelevant to these morphologies. Both the time scales of development and the spatial scales of expression can be expected to differ depending on whether the flow is laminar or turbulent; this is because laminar and turbulent flows obey different friction relations, one is Reynolds dependent and the other is not. In addition, there is a class of morphologies and morphodynamic phenomena, typically associated with the turbulent suspension of sediment that cannot be modelled in laminar flow.

Having said the above, the range of fluvial morphologies that can be created by laminar flow, and their general correspondence to their analogues created by turbulent flow, is notable. Based on this, and based on the common physical basis for both types of morphodynamics, it is concluded that microscale experiments using laminar flow can provide a relatively quick and inexpensive way to obtain insights into many aspects of fluvial morphodynamics.

In closing, the present authors would add that the body of research cited here constitutes only a subset of the available literature on laminar morphodynamics. Laminar flows have been used, for example, to model drainage basin evolution (Hasbargen & Paola, 2000), the response of delta to base-level change (Muto, 2001) or even the response of the drainage network to tectonic uplift (Lague *et al.*, 2003). Similarly, river avulsion and the formation of large-scale distributaries on fans and deltas do not appear to depend fundamentally on turbulence but are controlled primarily by the time scales of bank erosion and channel deposition (Jerolmack & Mohrig, 2007; Hoyal & Sheets, 2009).

ACKNOWLEDGEMENTS

We thank Y. Gamblin and A. Vieira of the Institut de Physique du Globe de Paris for their technical assistance in designing and realizing the experimental set-ups. We are also indebted to C. Jaupart, O. Devauchelle and M. Tal for many fruitful discussions. We gratefully acknowledge the insightful comments of C. Paola, D. Jerolmack and of the anonymous referees, which served to improve the paper.

The participation of Cantelli and Parker in this joint effort was made possible by the National Center for Earth Surface Dynamics (NCED), a centre funded by the Science and Technology Center program of the US National Science Foundation under agreement EAR-0120914. This paper represents a contribution to the effort of NCED in the area of channels. Cantelli and Parker also gratefully acknowledge the support of Shell Oil. The contribution to this joint effort from the University of Auckland (Coleman) was funded by the Marsden Fund (UOA220), administered by the Royal Society of New Zealand.

REFERENCES

Ackers, P. (1964) Experiments on small streams in alluvium. *J. Hydraul. Eng.*, **90,** 1–37.

Anderson, A.G. (1953) The characteristics of sediment waves formed by flow in open channels. *Proceedings, 3rd Midwest Conference on Fluid Mechanics*. PhD thesis. University of Minnesota, Minneapolis, MN, pp. 379–395.

Armstrong, L. (2003) *Bank erosion and sediment transport in a microscale straight river*. Doctoral thesis, Université Paris 7, Denis Diderot, France.

Ashworth, P.J., Bennett, S.J., Best, J.L. and **McLelland, S.J.** (1996) *Coherent Flow Structures in Open Channels*. Wiley, London, 733 pp.

Blondeaux, P. and **Seminara, G.** (1985) A unified bar-bend theory of river meanders. *J. Fluid Mech.*, **112,** 363–377.

Carling, P.A., Richardson, K. and **Ikeda, H.** (2005) A flume experiment on the development of subaqueous fine-gravel dunes from a lower-stage plane bed. *J. Geophys. Res. Earth Surf.*, **110** (F04S), 05–[15 pp], doi: 10.1029/2004JF000205.

Coleman, S.E. and **Eling, B.** (2000) Sand wavelets in laminar open-channel flows. *J. Hydraul. Res.* **38,** 331–338.

Coleman, S.E., Eling, B. and **Twose, G.** (1998) Sand-wave formation in laminar open-channel flow. In: *Proceedings of the Seventh International Symposium on River Sedimentation* (Eds A.W. Jayawardena, J.H.W. Lee and Z.Y. Wang), Hong Kong, China, 16–18 December, 73–78. Balkema, Rotterdam, ISBN 90 5809 0345.

Coleman, S.E., Fedele, J.J. and **Garcia, M.H.** (2003) Closed-conduit bed-form initiation and development. *J. Hydraul. Eng.* **129,** 956–965.

Davies, T.R.H., McSaveney, M.J. and **Clarkson, P.J.** (2003) Anthropic aggradation of the Waiho River, Westland, New Zealand: microscale modeling. *Earth Surf. Proc. Land.* **28,** 209–218.

Dean, W.R. (1928) The stream-line motion of fluid in a curved pipe. *Phil. Mag.* **5,** 673–695.

Devauchelle, O., Josserand, C., Lagrée, P.Y. and **Zaleski, S.** (2007) Morphodynamic modeling of erodible laminar channels. *Phys. Rev. E* **76,** 056318.

Diplas, P. (1990) Characteristics of self-formed straight channels. *J. Hydraul. Eng.* **116,** 707–728.

Einstein, A. (1926) The cause of the formation of meanders in the courses of rivers and of the so-called Baer's Law. *Die Naturwiss.*, **14,** 223–224.

Engelund, F. (1970) Instability of erodible beds. *J. Fluid Mech.* **42,** 225–244.

Engelund, F. (1974) Flow and bed topography in channel bends. *J. Hydraul. Eng.*, **100,** 1637–1648.

Engelund, F. and **Fredsøe, J.** (1982) Sediment ripples and dunes. *Annu. Rev. Fluid Mech.* **14,** 13–37.

Engelund, F. and **Hansen, E.** (1967) *A Monograph on Sediment Transport*. Technisk Forlag, Copenhagen, Denmark.

Federici, B. and **Paola, C.** (2003) Dynamics of channel bifurcations in noncohesive sediments. *Water Resour. Res.* **39,** 1–15.

Foley, M.G. and **Vanoni, V.A.** (1977) Pulsing flow in steep alluvial streams. *J. Hydraul. Eng.* **103,** 843–850.

Fredsøe, J. (1974) On the development of dunes in erodible channels. *J. Fluid Mech.* **64,** 1–16.

Gaines, R.A. and **Mainord, S.T.** (2001) Microscale loose-bed hydraulic models. *J. Hydraul. Eng.* **27,** 335–339.

Garcia, M.H. (2008) Sedimentation engineering. American Society of Civil Engineers Manual No. 110, Sedimentation Engineering: Processes, Measurements, Modeling, and Practice, ISBN 10 # 0784408149, ISBN 13 # 978078440814, 1050 pp.

Hasbargen, L.E. and **Paola, C.** (2000) Landscape instability in an experimental drainage basin. *Geology*, **28,** 1067–1070.

Hong, L.B. and **Davies, T.R.H.** (1979) A study of stream braiding. *Geol. Soc. Am. Bull.* **90,** 1094–1095.

Hoyal, D.C.J.D. and **Sheets, B.A.** (2009) Morphodynamic evolution of experimental cohesive deltas. *J. Geophys. Res.*, **114,** F02009, doi: 10.1029/2007JF000882.

Ikeda, S. (1981) Self-formed straight channels in sandy beds. *J. Hydraul. Eng.* **107,** 389–406.

Jerolmack, D.J. and **Mohrig, D.** (2007) Conditions for branching in depositional rivers. *Geology*, **35,** 463–466, doi: 10.1130/G23308A.1.

Johannesson, H. and **Parker, G.** (1989) Velocity redistribution in meandering channels. *J. Hydraul. Eng.*, **115,** 1019–1040.

Johnson, S., Cantelli, A., Pirmez, C. and **Parker, G.** (2008). *Experiments on Laminar Turbidity Currents*. Project Report No. 518, St. Anthony Falls Laboratory, University of Minnesota, Minneapolis, USA.

Kantha, L.H. and **Clayton, C.A.** (2000) *Small Scale Processes in Geophysical Flows*. Academic Press, San Diego, CA, 888 pp.

Kennedy, J.F. (1963) The mechanics of dunes and antidunes in erodible bed channels. *J. Fluid Mech.*, **16,** 521–544.

Keulegan, G.H. (1938) Laws of turbulent flow in open channels, National Bureau of Standards Research Paper RP 1151, USA.

Kikkawa, H., Ikeda, S. and **Kitagawa, A.** (1976) Flow and bed topography in curved open channels. *J. Hydraul. Eng.*, **102,** 1327–1342.

Kuroki, M. and **Kishi, T.** (1984) Regime criteria on bars and braids in alluvial straight channels. *Proc. Jpn Soc. Civ. Eng.*, **342,** 87–96.

Kuru, W.C., Leighton, D.T. and **McCready, M.J.** (1995) Formation of waves on a horizontal erodible bed of particles. *Int. J. Multiphase Flow* **21,** 1123–1140.

Lague, D., Crave, A. and **Davy, P.** (2003) Laboratory experiments simulating the geomorphic response to tectonic uplift. *J. Geophys. Res.*, **108,** 2008, doi: 10.1029/2002JB001785.

Lancien, P. (2007) *Experimental investigation of submarine channels*, Doctoral thesis, Institut de Physique du Globe de Paris, France.

Lancien, P., Lajeunesse, E. and **Métivier, F.** (2007) Near-wall velocity measurements by particle-shadow tracking. *Exp. Fluids* **42,** 843–846.

Liu, H.D. (1957) Mechanics of sediment ripple formation. *J. Hydraul. Res.*, **83,** 1197-1–1197-23.

Macky, G.H. (1999) Large flume experiments on the stable straight gravel bed channel. *Water Resour. Res.* **35,** 2601–2603.

Malverti, L., Lajeunesse, E. and **Métivier, F.** (2008) Small is beautiful: upscaling from microscale laminar to natural turbulent rivers. *J. Geophys. Res. Earth Surf.*, **113,** 14, doi: 10.1029/2007JF000974.

Métivier, F. and **Meunier, P.** (2003) Input and output mass flux correlations in an experimental braided stream. Implications on the dynamics of bed load transport. *J. Hydrol.* **271,** 22–38.

Métivier, F., Lajeunesse, E. and **Cacas, M.-C.** (2005) Submarine canyons in the bathtub. *J. Sed. Res.*, **75,** 6–11.

Meunier, P. and **Métivier, F.** (2000) Permanence des flux de masse dans une rivière en tresses expérimentales. *CR Acad. Sci. Paris Sciences de la Terre et des Planètes/Earth Planet. Sci.* **331,** 105–110.

Meyer-Peter, E. and **Müller, R.** (1948) Formulas for bed-load transport. *Proceedings of the 2nd Meeting, IAHR, Stockholm, Sweden*, 39–64.

Murray, A.B. and **Paola, C.** (1994) A cellular model of braided rivers. *Nature*, **371,** 54–57.

Muto, T. (2001) Shoreline autoretreat substantiated in flume experiment. *J. Sed. Res.*, **71,** 246–254.

Nezu, I. and **Nakagawa, H.** (1993) *Turbulence in Open-Channel Flows*. A.A. Balkema, Rotterdam, The Netherlands.

Parker, G. (1975) Sediment inertia as a cause of river antidunes. *J. Hydraul. Eng.*, **101,** 211–221.

Parker, G. (1976) On the cause and characteristic scales of meandering and braiding in rivers. *J. Fluid Mech.*, **76,** 457–480.

Parker, G. (1978) Self-formed straight rivers with equilibrium banks and mobile bed. Part 2. The gravel river. *J. Fluid Mech*. **89,** 127–146.

Parker, G., Fukushima, Y. and **Pantin, H.M.** (1986) Self accelerating turbidity currents. *J. Fluid Mech.*, **171,** 145–181.

Parker, G., Toro-Escobar, C.M., Ramey, M. and **Beck, S.** (2003) The effect of floodwater extraction on the morphology of mountain streams. *J. Hydraul. Eng.* **129,** 885–895.

Parker, G., Wilcock, P.R., Paola, C., Dietrich, W.E. and **Pitlick, J.** (2007) Quasi-universal relations for bankfull hydraulic geometry of single-thread gravel-bed rivers. *J. Geophys. Res. Earth Surf.*, **112,** 21, F04005, doi: 10.1029/2006JF000549.

Peakall, J. and **Warburton, J.** (1996) Surface tension in small hydraulic river models – the significance of the Weber number. *J. Hydrol. (New Zealand)*, **35,** 199–212.

Pirmez, C. and **Flood, R.D.** (1995) Morphology and structure of Amazon channel. In: *Proceedings of the ODP, Initial Reports, Vol. 155* (Eds R.D. Flood, D.J.W. Piper and A. Klaus), 23–45. Ocean Drilling Program, College Station, TX.

Pope, S.B. (2000) *Turbulent Flows*. Cambridge University Press, Cambridge, UK, 771 pp.

Reynolds, O. (1894) On the dynamical theory of incompressible viscous flows and the determination of the criterion. *Phil. Trans. Roy. Soc. London Ser. A* **174,** 935–982.

Reynolds, A.J. (1974) *Turbulent Flows in Engineering*. John Wiley and Sons, London, UK, 462 pp.

Rozovskii, I.L. (1961) *Flow of Water in Bends of Open Channels*. Israel Program for Scientific Translation, OTS 60-51133 (translator **Y.** Prushansky). Office of Technical Service, US Department of Commerce, Washington, DC, originally published by Academy of Sciences of the Ukraine SSR, 1957, 233 pp.

Schlichting, H. (1968) *Boundary-Layer Theory*, 6th edn. McGraw-Hill, New York, 748 pp.

Seminara, G. (2006) Meanders. *J. Fluid Mech.* **554,** 271–297.

da Silva, A. (2006) On the initiation of meandering and the subsequent plan-development of meander loops. *Proceedings of the Seventh International Conference on HydroScience and Engineering*, Drexel University, Philadelphia, USA, September 10–13, 17 pp. Available at : http://hdl.handle.net/1860/1496.

Smith, J.D. (1970) Stability of a sand wave subjected to shear flow of low Froude number. *J. Geophys. Res.* **75,** 5928–5940.

Smith, C.E. (1998) Modeling high sinuosity meanders in a small flume. *Geomorphology* **25,** 19–30.

Sun, T., Paola, C., Parker, G. and **Meakin, P.** (2002) Fluvial fan-deltas: linking channel processes with large-scale morphodynamics. *Water Resour. Res.*, **38,** 1151, doi: 10.1029/2001WR000284.

Tal, M. and **Paola, C.** (2007) Dynamic single-thread channels maintained by the interaction of flow and vegetation. *Geology* **35,** 347–350.

Tennekes, H. and **Lumley, J.L.** (1972) *A First Course in Turbulence*. MIT Press, Cambridge, MA.

Thompson, J. (1876) On the origin and winding of rivers in alluvial plains, with remarks on flow around bends in pipes. *Proc. Roy. Soc. London*, **25,** 5–8.

Vanoni, V. (1974) Factors determining bed forms of alluvial streams. *J. Hydraul. Eng.* **100,** 363–377.

Wong, M. and **Parker, G.** (2006) Reanalysis and correction of bed-load relation of Meyer–Peter and Müller using their own database. *J. Hydraul. Eng.* **132,** 1159–1168.

Yalin, M.S. (1992) *River Mechanics*. Pergamon Press, Inc., New York.

Yalin, M.S. and **da Silva, A.M.F.** (2001) *Fluvial Processes*. Monograph, International Association of Hydraulic Research. Kluwer, Delft, The Netherlands, 197 pp.

Yen, B.C. (1972) Spiral motion of developed flow in wide curved open channels. In: *Sedimentation* (Ed. H.W. Shen), chap. 22, 73–75, Colarado State Univ., Fort Collins, CO.

Yu, B., Cantelli, A., Marr, J., Pirmez, C., O'Byrne, C. and **Parker, G.** (2006) Experiments on self-channelized subaqueous fans emplaced by turbidity currents and dilute mudflows. *J. Sed. Res.*, **76,** 889–902.

Manuscript received 1 September 2008; revision accepted 2 September 2009

APPENDIX: UNIFIED FORMULATION FOR LAMINAR/TURBULENT SECONDARY FLOW IN BENDS

The case of secondary flow in river bends offers an example of the central thesis of this paper: when turbulent-flow and laminar-flow morphodynamics have the same physical basis, light can be shed on the other even if dynamic scaling is not satisfied. Here, this is illustrated by considering the flow only: the resulting morphodynamics of point-bar construction can be inferred by the reader.

The case considered here is the original configuration studied by Rozovskii (1961): equilibrium open-channel flow in a bend of constant centreline curvature R_c (see Fig. 12). The streamwise, transverse and upward-normal co-ordinates are denoted as s, n and z, respectively. The flow is steady and uniform in the streamwise direction and has vertical sidewalls. The channel width B is taken to be small compared with R_c, and channel centreline depth H_c is taken to be small compared with B, so that the following conditions prevail:

$$\frac{B}{R_c} \ll 1, \quad \frac{H_c}{R_c} \ll 1 \qquad \text{(A1a,b)}$$

The above assumptions allow for a linearized treatment of the secondary flow. The various solutions for secondary flow based on linearization in the literature (e.g. Rozovskii, 1961; Yen, 1972; Kikkawa *et al.*, 1976) all yield similar results. Here, the formulation of Engelund (1974) is used (see also Johannesson & Parker, 1989).

The effect of bend curvature is to cause superelevation of the water surface, so that the depth toward the outside of the bed is higher than that toward the inside of the bed. In a linearized formulation of the governing equations, this can be represented in terms of a constant transverse water surface slope S_{tw} (Fig. 12). The assumption (Eq. A1b) allows consideration of a large central region of the channel that is unaffected by the walls, within which both the primary flow velocity u_s and the secondary flow velocity u_n vary only in the upward-normal direction z.

With these simplifications, the governing equation for secondary flow reduces to the form:

$$\frac{u_s^2}{R_c} - gS_{tw} + \frac{1}{\rho}\frac{d\tau_{nz}}{dz} = 0 \qquad \text{(A2)}$$

where g denotes gravitational acceleration, ρ denotes water density and τ_{nz} denotes the n–z component of the shear stress. The physical meaning of this equation is as follows. The first term on the left-hand side denotes the centrifugal force per unit mass acting on the fluid, which drives the water outward (positive n direction). The second term expresses a deviatoric pressure force per unit water mass, which acts inward. The fundamental balance in bend flow is between these two terms. The first term, however, varies in the vertical, whereas the second term does not. The resulting difference drives secondary flow, which is expressed in terms of the third term on the left-hand side of Eq. A2.

In the case of laminar flow, the third term on the left-hand side of Eq. A2 takes the form:

$$\frac{1}{\rho}\frac{d\tau_{nz}}{dz} = \frac{1}{\rho}\frac{d}{dz}\left(\mu\frac{du_n}{dz}\right) = \nu\frac{d^2u_n}{dz^2} \qquad \text{(A3)}$$

where μ and ν denote the dynamic and kinematic viscosities of water, respectively. In the case of turbulent flow, the analyses of Rozovskii (1961), Yen (1972), Engelund (1974) and Kikkawa *et al.* (1976) all use a kinematic eddy viscosity ν_t, so that the third term on the left-hand side of Eq. A2 is represented as:

$$\frac{1}{\rho}\frac{d\tau_{nz}}{dz} = \frac{d}{dz}\left(\nu_t\frac{du_n}{dz}\right) \qquad \text{(A4)}$$

In the formulation of Engelund (1974) used here, eddy viscosity is taken to be constant.

Let U denote the depth-averaged primary flow velocity. A dimensionless local primary velocity T and dimensionless upward-normal coordinate ζ are defined as:

$$T = \frac{u_s}{U}, \quad \zeta = \frac{z}{H_c} \qquad \text{(A5a,b)}$$

Now let u_* denote the shear velocity of the primary flow, which is related to the bed shear stress τ_{bs} of the primary flow as:

$$u_* = \sqrt{\frac{\tau_{bs}}{\rho}} \qquad \text{(A6)}$$

Two friction coefficients are defined here; a standard coefficient C_f given as:

$$C_f = \left(\frac{u_*}{U}\right)^2 \qquad \text{(A7)}$$

and a dimensionless Chezy resistance coefficient C_z, given as:

$$C_z = \frac{U}{u_*} = C_f^{-1/2} \qquad \text{(A8)}$$

Let S denote the streamwise bed slope. As long as the primary flow is steady and uniform, the bed shear stress is given by the relation:

$$\tau_{bs} = \rho u_*^2 = \rho g H_c S \qquad \text{(A9)}$$

regardless of whether the flow is laminar or turbulent.

In the case of laminar flow, the relations for T and C_f are found to be:

$$T = 3\left(\zeta - \frac{1}{2}\zeta^2\right), \quad C_f = \frac{3}{Re} \qquad \text{(A10a,b)}$$

where:

$$Re = \frac{UH}{\nu} \qquad \text{(A11)}$$

denotes the Reynolds number of the flow. The dimensionless Chezy resistance coefficient C_z is then given from Eqs A8 and A10b as:

$$C_z = \left(\frac{Re}{3}\right)^{1/2} \qquad \text{(A12)}$$

Note that Eq. A10a defines a parabolic profile.

The standard assumption for the vertical profile of primary velocity in the case of turbulent open channel flow is the logarithmic law. Engelund (1974) justifies an alternative but very similar formulation, i.e. a parabolic relation with a slip velocity at the bed. In this formulation the eddy viscosity ν_t is given as:

$$\nu_t = \alpha u_* H_c, \quad \alpha = \frac{1}{3} \tag{A13a,b}$$

and the dimensionless primary flow velocity is given as:

$$T = \frac{\chi + \zeta - (1/2)\zeta^2}{\chi_1}, \quad \chi = \chi_1 - \frac{1}{3} \tag{A14a,b}$$

The parameter χ_1 in Eq. A14a,b is obtained from the friction coefficient as:

$$\chi_1 = \alpha C_f^{-1/2} = \alpha \times C_z \tag{A15}$$

where here C_f and C_z refer to values for turbulent flow. Turbulent flows in rivers at field scale fall into the turbulent rough regime, so that C_f is reasonably approximated by the Keulegan (1938) relation:

$$C_f^{-1/2} = C_z = 6 + 2{\cdot}5 \ln\left(\frac{H_c}{k_c}\right) \tag{A16}$$

where k_c is a composite roughness height including the effects of grain roughness and form drag associated with bedforms.

First to be considered here is the case of laminar flow. The secondary flow velocity is made dimensionless as follows:

$$\frac{u_n}{U} = \frac{UH_c}{\nu}\frac{H_c}{R_c} G = Re \frac{H_c}{R_c} G \tag{A17}$$

In addition, the transverse water surface slope is scaled as:

$$S_{tw} = \frac{U^2}{R_c g}\chi_{20} \tag{A18}$$

where χ_{20} is an as yet undetermined but order-one dimensionless coefficient. Substituting Eqs A3, A5b, A17 and A18 into Eq. A2, the following relation is obtained for laminar secondary flow:

$$0 = T^2 + \chi_{20} + \frac{d^2 G}{d\zeta^2} \tag{A19}$$

where T is specified by Eq. A10a. The relevant boundary and integral conditions are: (i) vanishing velocity at the bed; (ii) vanishing shear stress at the water surface; and (iii) a secondary flow that vanishes in the vertical average, i.e.:

$$G(0) = 0, \quad \left.\frac{dG}{d\zeta}\right|_0 = 0, \quad \int_0^1 G \, d\zeta = 0 \tag{A20a,b,c}$$

The solution to Eq. A19 subject to Eq. A20a,b,c is:

$$G = \int_0^\zeta \int_{\zeta'}^1 T^2 d\zeta'' d\zeta' - \chi_{20}\left(\zeta - \frac{1}{2}\zeta^2\right),$$
$$\chi_{20} = 3\int_0^1 \int_0^\zeta \int_{\zeta'}^1 T^2 \, d\zeta'' \, d'\zeta \, d\zeta = 1{\cdot}54 \tag{A21a,b}$$

In the case of turbulent flow the same scaling is used for S_{tw}, i.e. Eq. A18, but a very different scaling is used for the secondary flow u_n:

$$\frac{u_n}{U} = \frac{1}{\alpha}\frac{U}{u_*}\frac{H_c}{R_c} G = \frac{C_z}{\alpha}\frac{H_c}{R_c} G \tag{A22}$$

Substituting Eqs A4, A5b, A13a, A18 and A22 into Eq. A2, it is found that the equation governing the secondary flow is identical to that obtained for laminar flow, i.e. Eq. A14. In that equation, however, T is specified according to Eq. A14 for turbulent flow. The boundary condition of vanishing shear stress at the water surface (Eq. A20b) and the integral condition (Eq. A20c) also apply to turbulent flow. In the Engelund formulation, however, the necessity to satisfy the friction relation Eq. A16 requires the use of a slip velocity at the bed. As a result, Eq. A20a is replaced by the condition:

$$G(0) = \chi \left.\frac{dG}{d\zeta}\right|_0 \tag{A23}$$

(Engelund, 1974; Johannesson & Parker, 1989). The solution to Eq. A19 subject to Eqs A20b,c and A23 is:

$$G = \int_0^\zeta \int_{\zeta'}^1 T^2 \, d\zeta'' \, d\zeta' + \chi \int_0^1 T^2 \, d\zeta - \chi_{20}\left(\chi + \zeta - \frac{1}{2}\zeta^2\right),$$
$$\chi_{20} = \frac{\int_0^1 \int_0^\zeta \int_{\zeta'}^1 T^2 \, d\zeta'' \, d\zeta' \, d\zeta + \chi \int_0^1 T^2 \, d\zeta}{\chi + (1/3)} \tag{A24a,b}$$

The common physical basis of laminar and turbulent secondary flow can be made apparent by comparing the relations for the dimensionless primary flow T (Eq. A10a for laminar flow and Eq. A14a,b for turbulent flow) and the dimensionless secondary flow G and dimensionless superelevation χ_{20} (Eq. A21a,b for laminar flow and

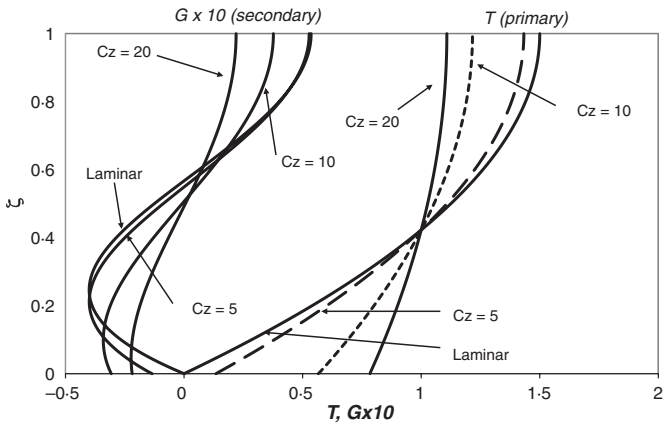

Fig. A1. Dimensionless primary and secondary flow velocities T and G, respectively, as functions of dimensionless vertical co-ordinate ζ. The plot shows results for laminar flow, and turbulent flows with C_z = 5, 10 and 20.

Eq. A24a,b for turbulent flow). Not only are the forms mathematically similar but, in addition, the solution for turbulent flow converges precisely with that for laminar flow in the limit as $\chi \to 0$.

A common range for C_z in rivers at bankfull flow is 5 to 20 (e.g. Parker *et al.*, 2007). Figure A1 shows plots of T (primary flow) and G (secondary flow) for laminar flow, as computed from Eq. A21a, and also for turbulent flow with C_z = 5, 10 and 20, as computed from Eq. A24a. It is seen directly from the figure that, whether the flow is laminar or turbulent, G has the same structure and the same order of magnitude. The effect of turbulence, however, can be discerned in the figure. The larger the value of C_z, the more effective turbulence is in mixing streamwise momentum in the vertical direction, so rendering the primary flow more uniform in the vertical and so weakening the strength of the secondary flow compared with laminar conditions.

Although the structure and order of magnitude of G is the same whether the flow is laminar or turbulent, the two cases do not scale with each other. In the case of laminar flow, it is seen from Eq. A17 that the ratio u_n/U varies linearly with the Reynolds number. In the case of hydraulically rough turbulent flow, for which C_z is Reynolds independent, it is seen from Eq. A22 that u_n/U is also Reynolds independent.

The fact that Reynolds scaling is not satisfied implies by no means that the two cases of secondary flow are fundamentally dissimilar; they proceed from the same physics and, when scaled appropriately, yield similar solutions for dimensionless secondary flow velocity G as a function of ζ. The analogy goes even further. Table 1 summarizes two cases for bend flow in a turbulent river; a turbulent field-scale case and a laminar microscale case. The field-scale case is based on estimates of parameters that fall within the range of gravel-bed rivers studied by Parker *et al.* (2007). The values for the microscale case are in the same range as those presented in Fig. 8. Let G_s and u_{ns} denote the surface values of G and u_n. In the case of the turbulent river flow, values of B, H_c, R_c, U and S are specified, and the dimensionless parameters H_c/B, H_c/R_c, Re, C_z, S, G_s, u_{ns}/U and Froude number Fr are computed using the relations Eqs A6, A7, A9, A22 and A24a,b, and the definition:

$$Fr = \frac{U}{\sqrt{gH_c}} \tag{A25}$$

In the case of laminar flow, B, H_c, R_c and U are specified, and the dimensionless parameters H_c/B, H_c/R_c, Re, C_z, S, G_s, u_{ns}/U and Fr are computed using Eqs A9, A11, A12, A17, A21a,b and A25, and an assumed value of $1{\cdot}00 \times 10^{-6}$ for the kinematic viscosity of water.

The results of the comparison shown in Table 1 are interpreted in the section headed: *Tea leaves and channel bends: flows with the same underlying physics need not be dynamically similar.*